THE JOURNAL OF BIOLOGICAL CHEMISTRY VOL. 291, NO. 41, pp. 21335–21349, October 7, 2016
Published in the U.S.A.

Structural Basis for Interactions Between Contactin Family Members and Protein-tyrosine Phosphatase Receptor Type G in Neural Tissues*[S]

Received for publication, June 6, 2016, and in revised form, August 10, 2016 Published, JBC Papers in Press, August 18, 2016, DOI 10.1074/jbc.M116.742163

Roman M. Nikolaienko[‡], Michal Hammel[§], Véronique Dubreuil[¶‖], Rana Zalmai[‡], David R. Hall[‡], Nurjahan Mehzabeen[‡], Sebastian J. Karuppan[‡], Sheila Harroch[‖1], Salvatore L. Stella[2], and Samuel Bouyain[‡3]**

*From the [‡]Division of Molecular Biology and Biochemistry, School of Biological Sciences, University of Missouri-Kansas City, Kansas City, Missouri 64110, the [§]Life Sciences Division, Lawrence Berkeley National Laboratory, Berkeley, California 94720, the [¶]Département de Neuroscience, Institut Pasteur de Paris, 25–28 Rue du Dr. Roux, 75624 Paris, France, [‖]Université Paris Diderot, Sorbonne Paris Cité, Epigenetics and Cell Fate, UMR 7216, CNRS, Paris, France, and the **Department of Basic Medical Science, University of Missouri-Kansas City School of Medicine, Kansas City, Missouri 64108*

Protein-tyrosine phosphatase receptor type G (RPTPγ/PTPRG) interacts *in vitro* with contactin-3–6 (CNTN3–6), a group of glycophosphatidylinositol-anchored cell adhesion molecules involved in the wiring of the nervous system. In addition to PTPRG, CNTNs associate with multiple transmembrane proteins and signal inside the cell via *cis*-binding partners to alleviate the absence of an intracellular region. Here, we use comprehensive biochemical and structural analyses to demonstrate that PTPRG·CNTN3–6 complexes share similar binding affinities and a conserved arrangement. Furthermore, as a first step to identifying PTPRG·CNTN complexes *in vivo*, we found that PTPRG and CNTN3 associate in the outer segments of mouse rod photoreceptor cells. In particular, PTPRG and CNTN3 form *cis*-complexes at the surface of photoreceptors yet interact in *trans* when expressed on the surfaces of apposing cells. Further structural analyses suggest that all CNTN ectodomains adopt a bent conformation and might lie parallel to the cell surface to accommodate these *cis* and *trans* binding modes. Taken together, these studies identify a PTPRG·CNTN complex *in vivo* and provide novel insights into PTPRG- and CNTN-mediated signaling.

The complex processes that shape the nervous system include the proliferation, differentiation, and migration of neural cells, axon guidance, and the formation of synapses. At the molecular level, these intricate processes rely on interactions between cell surface receptors coupled to intracellular downstream signaling networks. Such receptors might include cadherins, Ig superfamily proteins, neurexins, neuroligins, and leucine-rich repeat proteins as well as receptor tyrosine kinases and receptor protein-tyrosine phosphatases (RPTPs)[4] (1, 2). Members of the RPTP family typically combine large extracellular segments and intracellular phosphatase domains, which makes them ideally suited to coordinate cell adhesion and cell signaling. Among these, the homologous protein-tyrosine phosphatase receptor type G (PTPRG) and protein-tyrosine phosphatase receptor type Z (PTPRZ) were among the first RPTPs identified in the nervous system, and their ectodomains are characterized by the presence of an inactive N-terminal carbonic anhydrase-like (CA) domain that mediates protein-protein interactions (Fig. 1*A*) (3, 4). PTPRZ and its binding partner, the neural cell adhesion molecule contactin-1 (CNTN1), control the proliferation of oligodendrocyte precursor cells and their maturation into myelinating oligodendrocytes (5). Less is known, however, about PTPRG, its *in vivo* ligands, and the physiological roles these complexes might play.

Unlike PTPRZ, PTPRG is mostly expressed on neurons, although it has recently been found in some astrocytes and microglia in adult mouse brains (4, 6). PTPRG interacts *in vitro* via its CA domain with four homologs of CNTN1 called CNTN3–6 (7). All CNTNs are linked to the membrane by a glycophosphatidylinositol (GPI) anchor, suggesting that they require a co-receptor to signal across the membrane (8, 9). CNTNs are ubiquitously expressed in the nervous system and found predominantly on neurons. Over the years, CNTN3–6 have repeatedly been associated with the sensory circuitry. For example, CNTN3–5 are expressed in neuronal layers of chick embryo retinas (10). Furthermore, CNTN4 is expressed by axons of specific retinal ganglion cells to target the accessory optic system (11). It is also found on olfactory sensory neurons and guides their axons to specific glomeruli of the olfactory

* This work was supported by NIGMS, National Institutes of Health, Grant R01GM088806 (to S. B.). The authors declare that they have no conflicts of interest with the contents of this article. The content is solely the responsibility of the authors and does not necessarily represent the official views of the National Institutes of Health.

The atomic coordinates and structure factors (codes 5E5R, 5E5U, 5E4I, 5E53, 5E7L, 5E4Q, 5I99, 5E4S, 5E52, and 5E55) have been deposited in the Protein Data Bank (http://wwpdb.org/).

[S] This article contains supplemental Tables S1 and S2 and Figs. S1–S6.

[1] Present address: Dept. of Psychiatry, New York University School of Medicine, 550 First Ave., New York, NY 10016.

[2] Present address: Dept. of Neural and Behavioral Sciences, Penn State University College of Medicine, 500 University Dr., Hershey, PA 17033.

[3] To whom correspondence should be addressed: Division of Molecular Biology and Biochemistry, School of Biological Sciences, University of Missouri-Kansas City, 5100 Rockhill Rd., Kansas City, MO 64110. Tel.: 816-235-2658; E-mail: bouyains@umkc.edu.

[4] The abbreviations used are: RPTP, receptor protein-tyrosine phosphatase; PTPRG and PTPRZ, protein-tyrosine phosphatase receptor type G and Z, respectively; FN, fibronectin; CA, carbonic anhydrase-like; CNTN, contactin; GPI, glycophosphatidylinositol; ANOVA, analysis of variance; OS, outer segment; IS, inner segment; GCL, ganglion cell layer; PLA, proximity ligation assay; SAXS, small angle x-ray scattering; CNG, cyclic nucleotide-gated; PFA, paraformaldehyde; RMSD, root mean square deviation.

bulb, thus playing a role in odor map formation (12). CNTN5 is associated with the maturation of glutamatergic synapses of neurons of the auditory pathway (13), whereas CNTN6 participates in synapse formation between parallel fibers and Purkinje cells during cerebellar development (14). Less is known, however, about the physiological function of CNTN3, although *cntn3* transcripts have been detected in the granule cell layers of the olfactory bulb and Purkinje cells of the cerebellum (15). In broad terms, the sites and times of CNTN3–6 expression match those of PTPRG expression in sensory neurons, such as retinal ganglion cells, the cells of the glomerulus in the olfactory bulb, and ear sensory cells (4, 16). However, the formation of complexes between PTPRG and CNTN3–6 has yet to be confirmed *in vivo*. This has hampered our ability to define the potential biological roles of PTPRG·CNTN complexes.

Here, our crystallographic and biochemical analyses provide molecular insights into PTPRG·CNTN3 and PTPRG·CNTN6 complexes and indicate that PTPRG·CNTN complexes share a conserved arrangement. As a first step toward defining their potential physiological roles, we investigated the association of PTPRG and CNTN3 in mouse retinas. Notably, we identified PTPRG·CNTN3 complexes in the outer segments of adult mouse photoreceptors, suggesting that PTPRG·CNTN complexes form *in vivo*. Furthermore, our analyses reveal that the PTPRG·CNTN3 complex can form on the surface of a single photoreceptor cell, indicating that these two proteins form a *cis*-complex. This finding led us to consider the possibility that CNTNs might interact with PTPRG when expressed either on the same cell or on apposing cells. We thus wondered whether specific structural features in the extracellular regions of CNTNs could facilitate such interactions. Our crystallographic analyses indicate that the FN regions in CNTNs adopt a bent conformation that might place the ectodomains of CNTNs parallel to the cell surface, where they would bind to PTPRG in either *cis* or *trans* configurations. In a broader context, the sum of our analyses raises the possibility that PTPRG is a versatile signaling partner for CNTN3–6, possibly functioning as co-receptor when expressed on the same cell membrane and as a ligand when expressed on a distinct cell membrane.

Results

PTPRG Interacts Specifically with CNTN3–6—The results of previous affinity isolation assays using CNTN-transfected cells and a PTPRG resin suggested that the CA domain of PTPRG interacts with CNTN3–6, whereas the CA domain of the homologous PTPRZ interacts with CNTN1 only (7), yet it was important to test whether these interactions could occur on the surface of cells. We thus expressed the CA and FN domains of PTPRG as a fusion protein with human IgG Fc and applied it to HEK293 cells transfected with full-length CNTNs (Fig. 1, *A* and *B*). In these experiments, PTPRG-Fc fusion proteins bound to cells transfected with CNTN3–6 but not to cells transfected with CNTN1 or CNTN2, thus demonstrating that the ectodomain of PTPRG interacts specifically with CNTN3–6 expressed at the cell surface.

An earlier crystal structure of PTPRG(CA) bound to domains Ig1–Ig4 of mouse CNTN4 made it possible to identify CNTN4 residues that mediate interactions with PTPRG (7). Sequence analyses of CNTN3–6 indicate that these residues are strictly conserved, indicating that PTPRG·CNTN complexes may be arranged similarly. However, it remains unclear whether there might be quantitative differences among the interactions between PTPRG and full-length CNTN family members. To address this question, we designed a protein-protein binding assay utilizing AlphaScreen technology in which a luminescent signal is emitted when a biotinylated form of PTPRG(CA) attached to a donor bead associates with a full-length CNTN expressed as an Fc fusion protein bound to an acceptor bead (supplemental Fig. S1*A*) (17). The binding strength is measured indirectly in a competitive-binding assay format whereby a soluble form of PTPRG(CA) inhibits the interactions between the proteins immobilized on the beads (Fig. 1*C* and supplemental Table S1). The assays are thus conducted with a truncated PTPRG and dimerized CNTNs so that the IC_{50} values obtained are appropriate for comparing binding between PTPRG and CNTNs but might not, however, reflect the true binding constants between PTPRG and CNTNs expressed at the cell surface. Under these conditions, the IC_{50} values for PTPRG/CNTN interactions range from 235 nM (PTPRG/CNTN4) to 519 nM (PTPRG/CNTN6) and are similar to the IC_{50} value of 332 nM obtained for PTPRZ/CNTN1 (supplemental Fig. S1*B* and Table S1). One-way ANOVA statistics indicated that only IC_{50} differences measured for CNTN4 *versus* CNTN3 or CNTN6 and for CNTN5 *versus* CNTN6 were statistically significant (Fig. 1*D*). However, it remains unclear whether these variations in binding affinities are significant enough to suggest differences in the physiological roles of PTPRG·CNTN complexes.

A Conserved Arrangement of PTPRG/Z·CNTN Complexes—Previous work had demonstrated that the minimal PTPRG-binding site on CNTN3–6 comprises domains Ig2-Ig3 (7). Given the high level of sequence identity among CNTN3–6, we wondered whether there could remain differences in the details of the interactions between PTPRG and CNTN3–6. We addressed this by determining the co-crystal structures of PTPRG(CA) bound to the Ig2-Ig3 segments of CNTN3 and CNTN6 (Table 1 and Fig. 2, *A* and *B*). Overall, the crystal structures of the PTPRG·CNTN3 and PTPRG·CNTN6 complexes are similar to the structures of the PTPRG·CNTN4 and PTPRZ·CNTN1 complexes (5, 7) (Fig. 2*C*). The binding site includes a β-hairpin loop (residues 288–301) that contacts both Ig2 and Ig3 domains and a short stretch (residues 225–229) that interacts only with Ig3 (Fig. 2). The interface areas and shape complementarity coefficients are 1,668 $Å^2$/0.62 for the PTPRG·CNTN3 complex and 1,446 $Å^2$/0.68 for the PTPRG·CNTN6 complex. These values are comparable with the published values for the PTPRG·CNTN4 and PTPRZ·CNTN1 complexes. Overall, these analyses indicate that the complexes of PTPRG and PTPRZ bound to their cognate CNTN partners share a conserved arrangement with one another.

Broadly, interfaces for the PTPRG·CNTN complexes can be divided into four parts (Fig. 3, *A*–*D*): 1) a predominantly hydrophobic site that comprises residues on the base of the PTPRG(CA) β-hairpin loop; 2) a 5-amino acid stretch interacting with corresponding residues in the Ig3 domain of CNTN3/6; 3) an antiparallel β-sheet formed by the β-hairpin

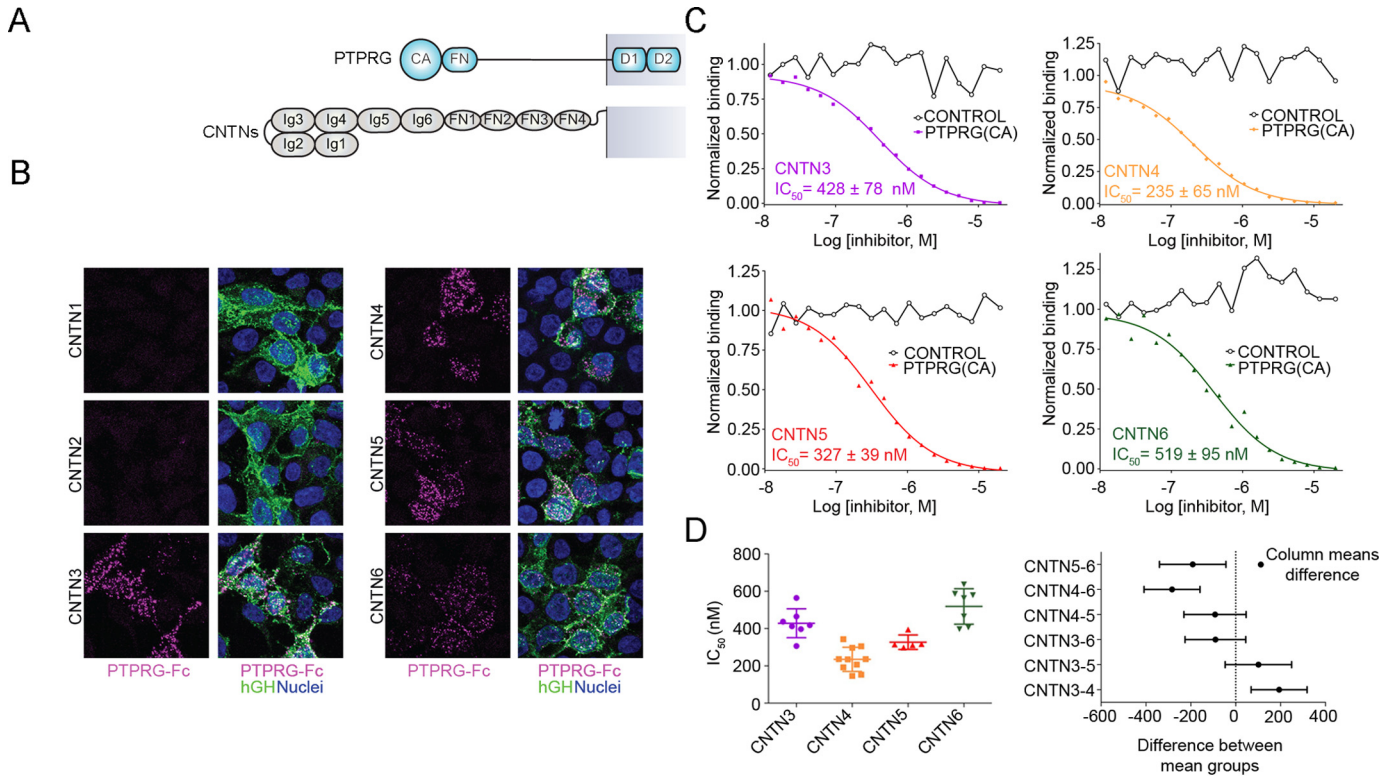

FIGURE 1. **PTPRG interacts specifically with CNTN3, -4, -5, and -6.** *A*, domain organization of PTPRG and CNTNs. PTPRG includes an inactive N-terminal CA domain, a single FN type III domain, a spacer region, and two intracellular tyrosine phosphatase domains. CNTNs include six Ig domains, four FN domains, and a GPI anchor. *B*, the extracellular domain of PTPRG associates with CNTN3–6 but not with CNTN1 or CNTN2. HEK293 cells transfected with full-length CNTNs fused to human growth hormone were incubated with an Fc fusion of the CA and FN domains of mouse PTPRG labeled with fluorescein isothiocyanate (*magenta*). CNTN-expressing cells were labeled with an antibody conjugated to a green fluorophore. The nuclei were visualized using DAPI. *C*, interactions between the CA domain of PTPRG with CNTN3–6, as determined by an AlphaScreen bead-based competition assay. The ability of mouse PTPRG(CA) or bovine CAII (control) to inhibit binding between an Fc fusion of full-length mouse CNTN3–6 and biotin-labeled PTPRG(CA) was assessed over a logarithmic dilution series. IC_{50} values are reported as averages ± S.D. (*error bars*) from at least three experiments. One representative experiment for each series is shown. See supplemental Table S1 for detailed results. *D*, one-way ANOVA analysis of the IC_{50} values measured in *C*. The means and S.D. values are shown on the graph on the *left*, whereas the graph on the *right* shows Tukey 99% confidence intervals for Tukey's multiple comparison tests. Differences between CNTN3 and CNTN4, CNTN4 and CNTN6, and CNTN5 and CNTN6 are statistically significant, whereas the remaining IC_{50} differences (between CNTN3 and CNTN5, CNTN3 and CNTN6, and CNTN4 and CNTN5) are not. See supplemental Fig. S1.

loop and an antiparallel three-strand β-sheet in domain Ig2 of CNTN3/6; and 4) the tip of the β-hairpin loop formed by residues Gln^{293}–Val^{296} that interacts with domain Ig2 of CNTN3/6. In the PTPRG·CNTN3/6 complexes, site 1 is formed by PTPRG residues Phe^{288}, Thr^{289}, Thr^{290}, and Tyr^{301} and CNTN3/6 residues Met^{222} and Tyr^{225}. Site 2 includes residues Val^{225}-Lys^{229} in PTPRG and residues Glu^{226}, Pro^{227}, Lys^{228}, and Asn^{306} in CNTN3/6. In site 3, the combined 5-strand antiparallel β-sheet is stabilized by hydrogen bonds between the main chain atoms of His^{295}–Glu^{300} in PTPRG and Gly^{139}–Leu^{143} in CNTN3/6. In addition, the side chain of CNTN3/6 Gln^{138} side chain forms two hydrogen bonds with the main chain atoms of Val^{299} and side chain atoms of Glu^{300} in PTPRG. Finally, in site 4, the tip of the PTPRG(CA) β-hairpin loop rests against the Ig2 domain of CNTN3/6, and the side chain of His^{295} packs against Arg^{129} in particular. Although the contacts found at sites 1–3 are conserved in all PTPRG·CNTN structures, the side chains of residues Gln^{293}, Asp^{294}, His^{295}, and Val^{296} in site 4 adopt distinct conformations (Fig. 3*D*), which suggests that this region is flexible and might only play a minor role in mediating protein-protein interactions. The conserved contacts at the interfaces of complexes formed by PTPRG with CNTN3, -4, and -6 (Fig. 3*E*) are consistent with the comparable IC_{50} values determined in our binding assays (Fig. 1, *C* and *D*). Finally, it was not possible to obtain co-crystals of PTPRG and CNTN5, but comparison of the PTPRG-binding site in CNTN4 and the corresponding region in CNTN5 shows that they are essentially identical (Fig. 3*F*). This finding, along with the similar affinities between PTPRG(CA) and CNTN3–6, strongly suggests that the binding mode observed for PTPRG(CA) and CNTN3, -4, and -6 is conserved for PTPRG and CNTN5.

Validation of the PTPRG·CNTN Interface—Although most of the interactions between PTPRG and its cognate CNTN partners are mediated by the β-hairpin loop in the CA domain of PTPRG (Fig. 3), comparison of the complexes PTPRG forms with CNTN3, -4, and -6 indicates that the tip of the loop adopts distinct conformations, arguing that it might not mediate essential contacts (Fig. 3*E*). We designed three mutant forms of the CA domain of mouse PTPRG to define the contribution of each region to the complex formation (Fig. 4*A*): 1) a deletion mutant in which sites 3 and 4 are eliminated as residues 290–299 of the β-hairpin loop are replaced by the tripeptide ASA; 2) a form including the mutations H295A/V296A at the tip of the β-hairpin in site 4; and 3) a form that includes two alanine mutations in the short loop in site 2 (H226A/K229A). All pro-

TABLE 1
Data collection and refinement statistics

	CNTN3(Ig2-Ig3)·PTPRG(CA)	CNTN6(Ig2-Ig3)·PTPRG(CA)	CNTN5(Ig1–Ig4)	CNTN1 (FN1–FN3)	SeCNTN2 (FN1–FN3)	CNTN2 (FN1–FN3)	CNTN3 (FN1-FN3)	CNTN3 (Ig5-FN2)	CNTN4 (FN1–FN3)	CNTN5 (FN1–FN3)	CNTN6 (FN1–FN3)
Data collection											
Beamline	APS 22-ID	APS 22-BM	APS 22-BM	APS 22-ID	APS 22-BM	APS 22-ID	APS 22-ID	APS 22-BM	APS 22-BM	APS 22-ID	APS 22-ID
Wavelength (Å)	1.0	1.0	1.0	1.0	0.97916	1.0	1.0	1.0	0.97933	1.0	1.0
Unique reflections	31,166	70,482	14,070	48,701	49,121	28,357	8,976	20,578	13,387	14,285	21,656
Resolution (Å)	50–2.6	50–2.0	50–2.6	50–2.5	50–1.8	30–2.0	50–2.8	50–2.4	50–2.5	50–2.7	50–2.7
Space group	$P2_12_12$	$P2_12_12_1$	C2	$P2_1$	$P2_12_12$	$P2_12_12$	C2	$P2_12_12_1$	$C222_1$	$C222_1$	$P2_12_12_1$
Unit cell											
a, *b*, *c* (Å)	74.14, 90.53, 147.45	78.64, 113.53, 117.05	179.98, 50.66, 51.02	87.48, 49.87, 163.30	124.82, 40.85, 83.11	124.39, 40.67, 82.60	185.10, 39.03, 52.40	58.22, 76.93, 115.82	94.79, 144.3, 55.40	83.77, 154.52, 90.42	86.74, 90.85, 99.35
α, β, γ (degrees)	90.0, 90.0, 90.0	90.0, 90.0, 90.0	90.0, 101.67, 90.0	90.0, 97.12, 90.0	90.0, 90.0, 90.0	90.0, 90.0, 90.0	90.0, 96.9, 90.0	90.0, 90.0, 90.0	90.0, 90.0, 90.0	90.0, 90.0, 90.0	90.0, 90.0, 90.0
R_{sym}[a]	0.134 (0.588)[b]	0.096 (0.593)	0.154 (0.435)	0.075 (0.380)	0.082 (0.479)	0.110 (0.508)	0.139 (0.377)	0.165 (0.548)	0.08 (0.460)	0.112 (0.418)	0.155 (0.515)
Completeness[b] (%)	99.6 (96.3)	98.7 (89.2)	98.8 (90.7)	99.2 (92.3)	99.1 (92.7)	97.8 (89.3)	97.7 (90.0)	98.2 (87.5)	98.3 (87.4)	85.7 (56.3)	97.9 (92.5)
Redundancy	11.4 (5.3)	7.1 (5.3)	6.5 (3.5)	6.9 (4.7)	7.0 (5.6)	5.9 (3.2)	8.9 (5.8)	11.9 (7.9)	6.1 (4.2)	12 (5.9)	7.4 (4.8)
$I/i\Sigma i$	7.2 (2.3)	19.5 (2.0)	11.4 (2.3)	20.4 (3.3)	19.8 (2.7)	12.5 (1.6)	15.0 (4)	14.8 (2.4)	20.7 (2.3)	17.35 (3.6)	8.4 (2.1)
Refinement											
Molecules in asymmetric unit	2 × 2	2 × 2	1	4		1	1	1	1	1	2
Resolution (Å)	49.2–2.6	24.9–2.0	37.0–2.6	43.5–2.5		29.1–2.0	47.8–2.8	43.1–2.4	28.7–2.5	38.6–2.7	43.4–2.7
R_{work}[c]/R_{free}	0.187/0.249	0.167/0.217	0.195/0.264	0.204/0.247		0.190/0.226	0.183/0.244	0.203/0.253	0.190/0.255	0.194/0.231	0.200/241
No. of atoms	7,291	8,039	3,086	9,572		2,491	2,135	3,190	2,394	2,282	4,715
Protein	7,205	7,392	2,968	9,267		2,301	2,110	3,032	2,325	2,258	4,672
Ligand	27	112	28	75				6		5	
Water	59	535	90	230		190	25	152	69	19	43
Root mean square deviations											
Ideal bonds (Å)	0.009	0.007	0.003	0.004		0.007	0.01	0.009	0.009	0.009	0.004
Ideal angles (degrees)	1.10	1.05	0.83	0.84		1.06	1.21	1.28	1.12	1.13	0.92
Average *B* factors (Å^2)	71.2	40.9	50.1	63.7		39.2	57	41.2	61.6	93.7	42.8
Protein	71.3	40.4	49.6	63.9		39.1	57.2	41.3	61.8	93.8	42.9
Ligand	98.3	71.9	88.0	85.5				62.9		121.1	
Water	49.9	41.6	51.6	50.2		40.5	38.9	36.9	53.5	69.7	34.9
Ramachandran statistics											
Favored (%)	94	97	95	96		98	95	96	97	94	97
Allowed (%)	6	3	5	4		2	5	4	3	6	3
PDB accession code	5E5R	5E5U	5E4I	5E53		5E7L	5E4Q	5I99	5E4S	5E52	5E55

[a] $R_{sym} = \Sigma_h \Sigma_i |I_i(h) - \langle I(h)\rangle| / \Sigma_h \Sigma_i I_i(h)$, where $I_i(h)$ is the *i*th measurement of reflection *h* and $\langle I(h)\rangle$ is a weighted mean of all measurements of *h*.
[b] Values in parentheses apply to the high resolution shell.
[c] $r = \Sigma_h F_o(h) - F_c(h) / \Sigma_h |F_o|$. R_{work} and R_{free} were calculated from the working and test reflection sets, respectively.

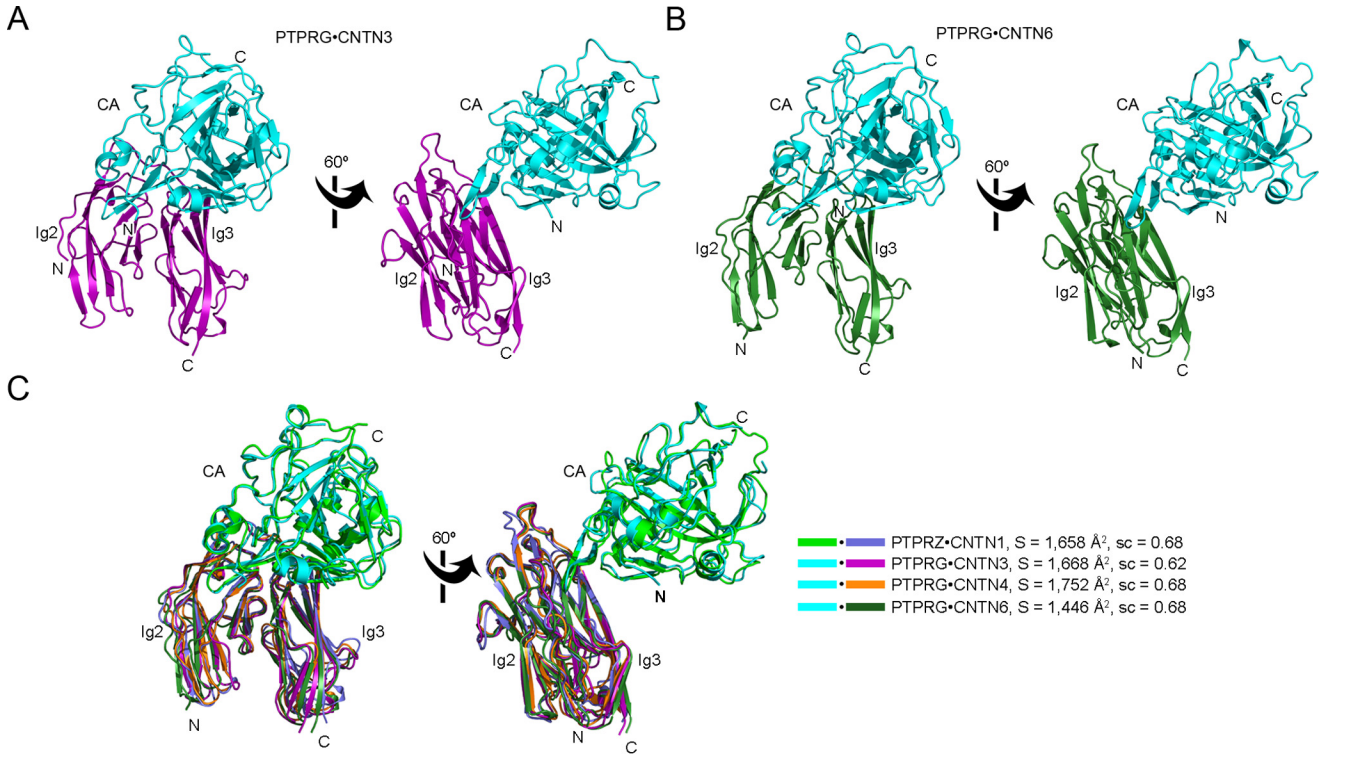

FIGURE 2. **A conserved arrangement of complexes formed by the CA domains of PTPRG/Z and domains Ig2-Ig3 of CNTNs.** The PTPRG(CA)·CNTN3(Ig2-Ig3) and PTPRG(CA)·CNTN6(Ig2-Ig3) complexes are shown in *ribbon diagrams* along with an overlay of all the complexes formed by PTPRG, PTPRZ, and their CNTN-binding partners. The CA domains of PTPRG and PTPRZ are *colored cyan* and *green*, respectively. Repeats Ig2-Ig3 of CNTN1, CNTN3, CNTN4, and CNTN6 are *colored slate*, *magenta*, *orange*, and *dark green*, respectively. *N* and *C*, N and C termini, respectively. *A*, the CA domain of PTPRG bound to the Ig2-Ig3 repeats of CNTN3. *B*, the CA domain of PTPRG bound to the Ig2-Ig3 repeats of CNTN6. *C*, structural comparison of the PTPRZ·CNTN1, PTPRG·CNTN3, PTPRG·CNTN4, and PTPRG·CNTN6 complexes. The complexes were superimposed by fitting domains Ig2-Ig3 of CNTN4 with the homologous repeats in CNTN1 (RMSD 1.27 Å over 186 equivalent Cαs), CNTN3 (RMSD 0.97 Å over 180 equivalent Cαs), and CNTN6 (RMSD 1.16 Å over 195 equivalent Cαs). The buried surface areas and the surface complementarity coefficients for each complex are shown beside the structure overlay.

teins behaved comparably with wild-type PTPRG(CA) and in particular were monomeric as determined by size exclusion chromatography. Furthermore, the structural integrity of the two alanine site-directed mutants was verified by circular dichroism spectropolarimetry, which indicates that the mutations did not alter the secondary structures of these mutated domains (supplemental Fig. S2). Because our analyses strongly suggest that all PTPRG·CNTN complexes share a similar binding mode, the binding activities of these mutant proteins were only tested for CNTN4 (Fig. 4*B*).

The β-hairpin deletion mutant did not inhibit the interaction between PTPRG(CA) and an IgG Fc fusion of mouse CNTN4, which mirrors the effect of the β-hairpin deletion on the binding of PTPRZ and CNTN1 (5). In contrast, the mutations H295A/V296A only increased the IC_{50} by ~4-fold, consistent with our observation that contacts in site 4 might not be essential for complex formation. The decrease in binding may result from the loss of the hydrophobic Val^{296} side chain, which interacts with CNTN Leu^{142} and Val^{132} in CNTN3, -4, and -6. Removing the His^{295} side chain prevents van der Waals contacts with the side chain atoms of Arg^{129} and Cys^{144}. However, one expects that the substitution to alanine residues would preserve the main chain interactions, including formation of the five-strand antiparallel β-sheet (Fig. 2*C*). Finally, mutating His^{226} and Lys^{229} to alanine abolished the CNTN4 binding activity (Fig. 4*B*). Indeed, His^{226} mediates conserved non-polar interaction with Tyr^{225}, Pro^{227}, and Lys^{228} and a hydrogen bond with the main-chain oxygen atom of Glu^{298}. Substituting Lys^{229} to alanine disrupts the Lys^{229}-Glu^{226} salt bridge and the Lys^{229}-Asn^{306} hydrogen bond (Fig. 3, *B* and *D*). Overall, these results confirm the importance of the β-hairpin loop in complex formation but also indicate that contacts located in site 2 mediate essential interactions at the interface.

Identification of a PTPRG·CNTN Complex in Adult Mouse Retina—Despite strong lines of evidence that PTPRG interacts specifically with CNTN3–6 *in vitro*, the identification of such complexes *in vivo* has yet to be investigated thoroughly. This question was addressed in mouse retinas, where PTPRG and CNTN3–5 are expressed (10, 16). In simple terms, the retina includes three major neuronal layers (Fig. 5*A*). Light is first detected by photopigments in the outer segments of rod and cone photoreceptor cells spanning the outer segment (OS), inner segment (IS), and outer nuclear layer. Information is then transmitted to the bipolar cells found in the inner nuclear layer and then to ganglion cells in the ganglion cell layer (GCL) before being sent to the visual cortex by the optic nerve. The outer plexiform layer and inner plexiform layer include synapses between the photoreceptors and bipolar cells and between the bipolar cells and ganglion cells, respectively.

As a first step, we analyzed the distribution of PTPRG and CNTN3 by immunohistochemistry using antibodies from commercial sources that we validated in our laboratory (Fig. 5*B* and supplemental Fig. S3, *A* and *B*). Consistent with previous findings (16), a strong signal could be observed for PTPRG in the

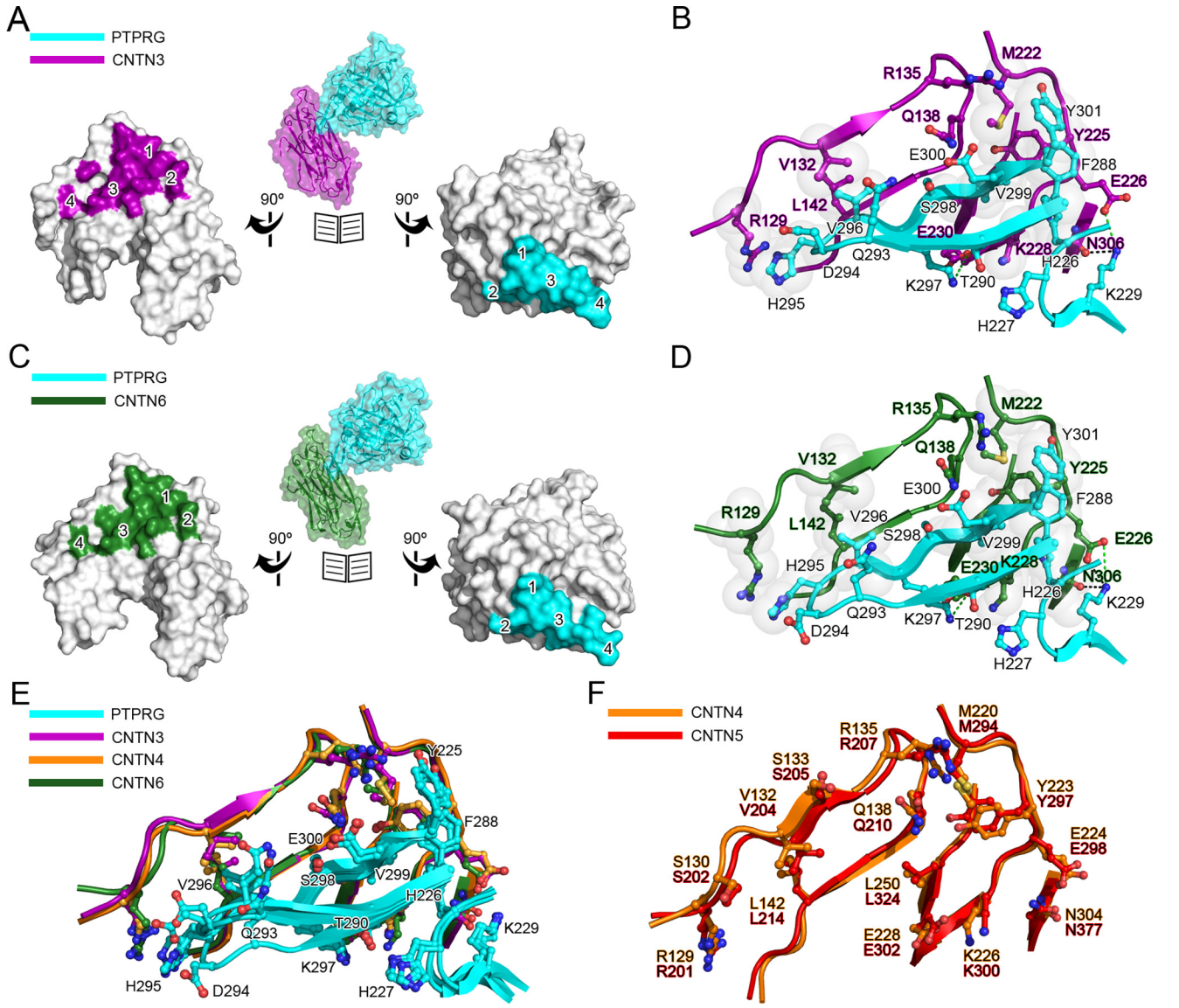

FIGURE 3. **Conserved interactions at the PTPRG·CNTN interfaces.** *A*, open book surface representation of the complex between the CA domain of PTPRG and CNTN3 repeats Ig2-Ig3. CNTN3 residues at the complex interface are *colored magenta*, whereas PTPRG residues are *colored cyan*. Binding sites 1–4 are labeled on the CNTN3 and PTPRG surfaces. *B*, detailed view of the PTPRG·CNTN3 interface. This view is in the same orientation as the ones shown on the *left* in Fig. 2. *Translucent gray spheres* highlight residues involved in van der Waals contacts. *Dashed lines* indicate potential hydrogen bonds (*black*) and salt bridges (*green*). *C* and *D*, same as *A* and *B*, but for the complex between the CA domain of PTPRG and CNTN6 repeats Ig2-Ig3. *E*, structural comparisons of the interfaces in the complexes formed by PTPRG and CNTN3, -4, and -6 (colored *cyan*, *magenta*, *orange*, and *dark green*, respectively). *F*, overlay of the PTPRG-binding region of mouse CNTN4 (*orange*) and mouse CNTN5 (*red*). The PTPRG-binding residues in CNTN4 are strictly conserved in CNTN5.

OSs, ISs, inner plexiform layer, and GCL. By contrast, CNTN3 was mostly localized to the OS, where it overlapped with PTPRG (Fig. 5*B*). We decided to assess whether PTPRG and CNTN3 form complexes in the OS by using an *in situ* proximity ligation assay (PLA) (18, 19). In these experiments, we detected the interaction of endogenous PTPRG and CNTN3 *in vivo* by using antibodies to determine whether these proteins are in close proximity with one another (<40 nm). Consistent with our immunohistochemistry experiments, a strong signal was observed in the OS of the photoreceptors, suggesting that PTPRG and CNTN3 form a complex in photoreceptors (Fig. 5*C*). In contrast, no signal was observed when the primary antibody against CNTN3 was omitted (Fig. 5*D*). Furthermore, we observed PLA spots in the OS when we conducted assays using a distinct PTPRG antibody raised against its CA domain, which confirms the specificity of the interactions identified between CNTN3 and PTPRG (supplemental Fig. S4).

Because our immunohistochemistry experiments indicated that PTPRG and CNTN3 are both expressed on photoreceptors, we wondered whether they could interact when expressed on the same cell (*cis*-interactions), because there are several examples of RPTPs forming *cis*-complexes with their ligands (20, 21). Thus, we dissociated rod photoreceptors from retinas to carry out *in situ* PLAs on solitary cells. As was the case for intact retinas, PLA spots indicating the presence of PTPRG·CNTN3 complexes were limited to the OS (Fig. 5*D*). Taken together, these results indicate that PTPRG and CNTN3 associate *in vivo* and suggest that these receptors can form *cis*-complexes. Taking into account the conserved interactions between the complexes formed by PTPRG and CNTN family members,

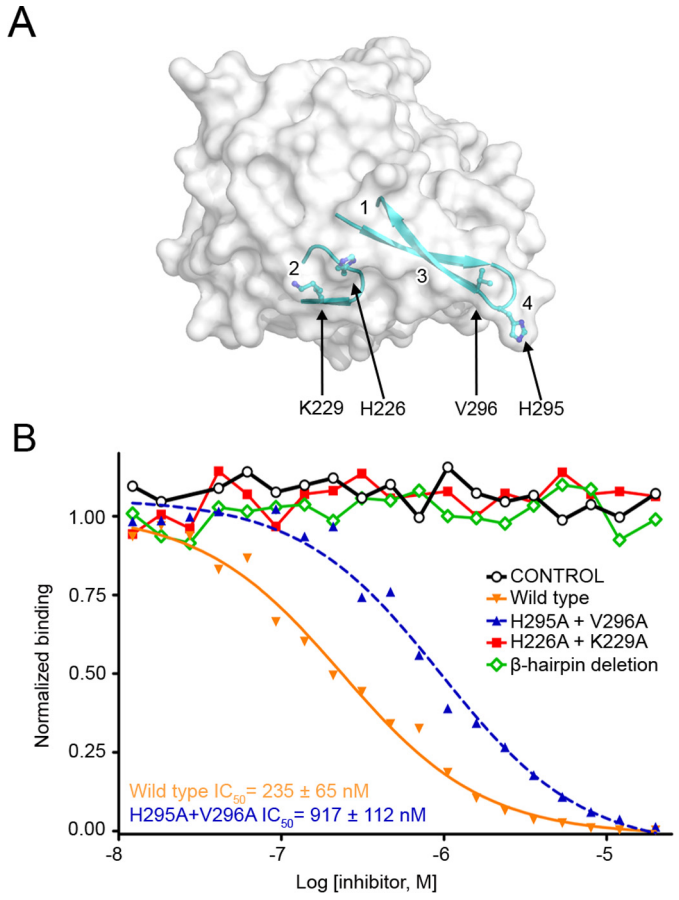

FIGURE 4. **Validation of the PTPRG·CNTN interface.** *A*, *surface representation* of the CA domain of PTPRG with the two loops responsible for CNTN binding shown in a *ribbon representation*. The residues mutated to alanine in the binding assays shown in *B* are shown as *ball-and-stick representations*. Binding sites 1–4 are *labeled* on the PTPRG surface. *B*, mutational analysis of interactions between the CA domain of PTPRG with CNTN4. The ability of bovine CAII (control), mouse PTPRG(CA), or mouse PTPRG(CA) mutants to inhibit binding between an IgG Fc fusion of mouse CNTN4 and a biotin-labeled PTPRG(CA) was assessed over a logarithmic dilution series. See supplemental Fig. S2.

we surmise that PTPRG might associate in *cis* with CNTN3–6 *in vivo*.

PTPRG and CNTN3 Also Form trans-Complexes—The discovery that PTPRG and CNTN3 can form *cis*-complexes left us wondering whether these cell surface receptors are limited to *cis*-interactions or could also interact when expressed on distinct cells (*trans*-interaction), as is the case for their respective homologs PTPRZ and CNTN1 (5, 22). Demonstrating such interactions would indicate that PTPRG and CNTNs might mediate specific interactions to enable selective neuronal connections during brain wiring. We thus designed a cell aggregation assay to investigate this possibility. We transiently transfected HEK293F cells with either mEmerald-CNTN1, mEmerald-CNTN3, or mCherry-PTPRG and assessed the formation of cellular aggregates after mixing these cell populations. Expression of CNTN1, CNTN3, or PTPRG did not induce cellular aggregation (Fig. 6, *A–C*), but *green* and *magenta* cell aggregates formed readily upon mixing of CNTN3- and PTPRG-expressing cells (Fig. 6, *E* and *F*). We did not observe such aggregates when CNTN1- and PTPRG-expressing cells were mixed (Fig. 6*D*), consistent with our finding that CNTN1 and PTPRG do not interact (Fig. 1*B*). Thus, these results suggest that PTPRG and CNTN3 interact when expressed on distinct cell surfaces. Taken together with the results of our PLAs on single photoreceptors (Fig. 5*D*), these findings strongly suggest that PTPRG and CNTN3 form *cis*- and *trans*-complexes.

The Conformation of the CNTN Ectodomain Is Compatible with cis- and trans-Complex Formation—We wondered how the conformations of the CNTN3 and PTPRG ectodomains could accommodate the formation of *cis*- and *trans*-complexes. The extracellular region of PTPRG includes a ~300-amino acid stalk between the FN domain and the transmembrane helix. This stalk does not include any recognizable structural motifs (23) save for *N*-linked and *O*-linked glycosylation sites and might thus provide enough flexibility to accommodate the two binding modes. In the case of CNTN3, on the other hand, we considered two possibilities. First, the ectodomain of CNTN3 might be flexible enough to support the *cis* and *trans* binding modes. Although the ectodomains of CNTNs do not include any obvious region that would provide flexibility other than the short linkers between individual Ig and FN domains, the extracellular region of PTPRS, whose architecture resembles that of the CNTN ectodomains, is flexible enough to form *cis*- and *trans*-complexes during axon growth and synapse formation (24). Second, CNTNs might adopt conformations in which their extracellular regions are parallel to the cell surface, thus making it possible to use a similar binding mode to associate with *cis* and *trans* ligands. Such conformations have been identified in cell surface receptors, such as NCAM2 and α-neurexin (25–27), which feature a sharp bend between two domains close to the membrane.

We thus undertook structural studies to characterize the regions of CNTNs outside of the first four Ig repeats to gain insights into the conformations of CNTNs. In our hands, fragments of CNTNs that include FN4 either aggregated or were unstable, so we limited our investigations to the Ig5-FN3 fragment. Although we were able to grow crystals of mouse CNTN3(Ig5-FN3), these did not diffract. Thus, we determined the crystal structure of the Ig5-FN2 segment of mouse CNTN3 (Table 1) and discovered that it adopts an extended conformation (Fig. 7). We also characterized the conformation of the FN1–FN3 region of CNTN3 (Table 1). Intriguingly, this fragment adopts an L-shaped conformation characterized by a sharp bend between domains FN2 and FN3 (Fig. 8*A*). This conformation is found in FN1–FN3 fragments of CNTN1, -2, -4, -5, and -6 crystallized in distinct lattices, indicating that it might be a conserved feature of all CNTN family members rather than an artifact of crystallization. To test this hypothesis, we analyzed the solution conformation of FN1–FN3 of CNTN3 by small angle x-ray scattering (SAXS). We limited our analysis to CNTN3 because our findings indicate that it forms *cis*- and *trans*-complexes with PTPRG. The experimental SAXS profile for CNTN3(FN1–FN3) matches closely to the theoretical scattering profile calculated using the crystal structure of CNTN3(FN1–FN3) ($\chi^2 = 1.77$; Fig. 8*B*). Furthermore, the crystal structure of CNTN3(FN1–FN3) corresponds to a molecular envelope calculated using the experimental scattering profile (Fig. 8*C*). Overall, this analysis demonstrates that the L-shaped conformation adopted by this fragment of CNTN3 mirrors its

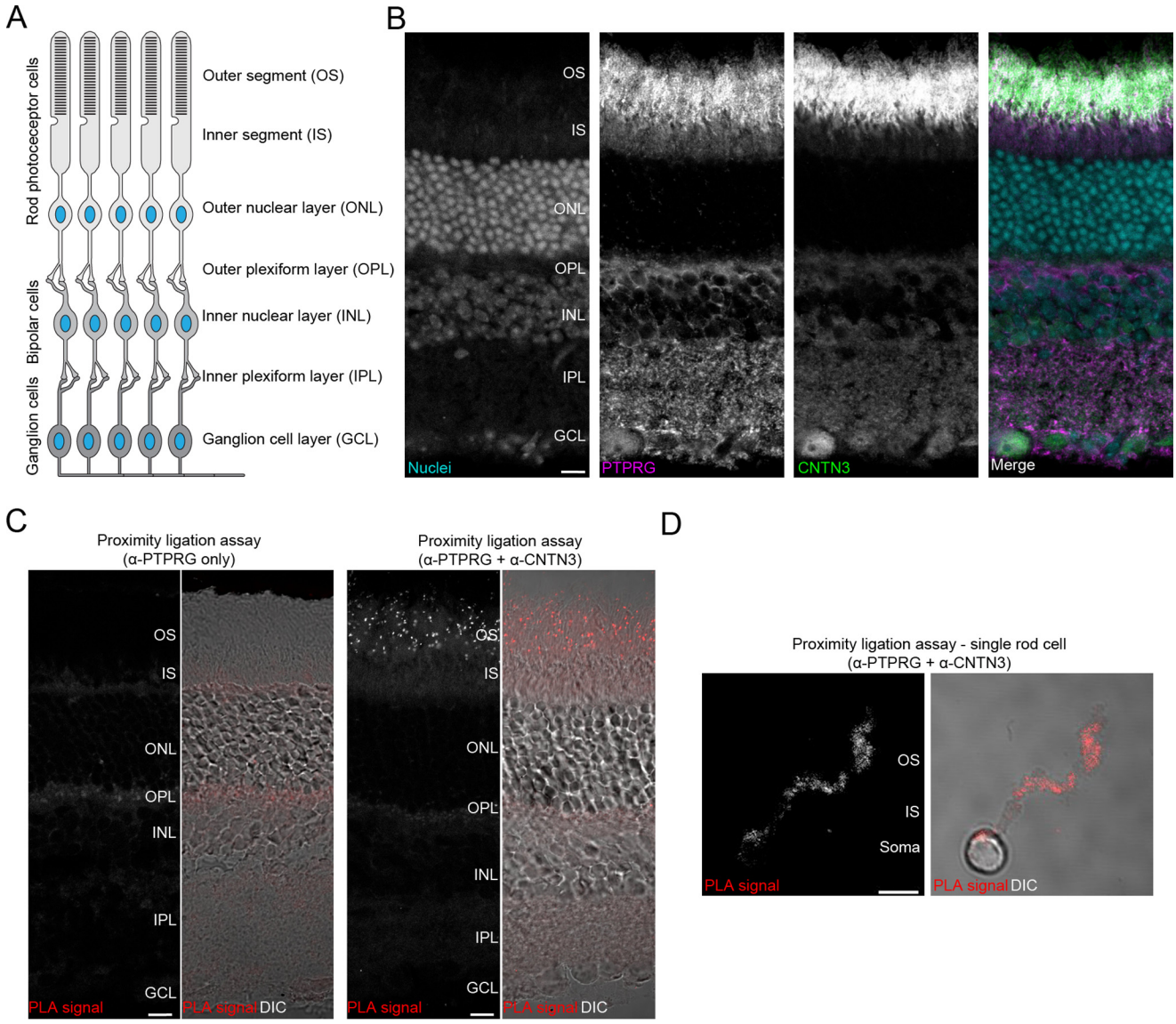

FIGURE 5. **Identification of the PTPRG·CNTN3 complex in the outer segments of adult mouse retinas.** *A*, schematic representation of the retinal architecture. Light information detected in an OS of a photoreceptor cell is eventually transmitted to cells in the GCL before being sent to the visual cortex by the optic nerve. *B*, PTPRG and CNTN3 both localize to the outer segments of adult mouse retinas. A retinal section was stained with antibodies against PTPRG or CNTN3. RedDot™ 1 staining was used to visualize nuclei. *Scale bar*, 10 μm. *C*, PTPRG and CNTN3 associate in the outer segments of photoreceptors. A PLA was performed to detect the presence of a PTPRG·CNTN3 complex. Omission of the primary antibody against CNTN3 did not yield any detectable signal (control, *left panels*), whereas introducing it revealed the presence of punctate staining indicative of PTPRG and CNTN3 being in close proximity in the OS. The *panel* with DIC (differential interference contrast) shows a more detailed view of the retinal organization. *Scale bar*, 10 μm. *D*, an *in situ* PLA performed on a single photoreceptor cell shows the presence of PTPRG·CNTN3 complexes on the same cell, suggesting that PTPRG and CNTN3 interact in *cis*. *Scale bar*, 5 μm. See supplemental Figs. S3 and S4.

conformation in solution. Taken together, these findings indicate that the FN regions of CNTNs all adopt a bent conformation reminiscent of the one adopted by NCAM2 (25).

Analysis of the residues found at the FN2-FN3 interfaces in CNTN1–6 indicates that the bent conformation is stabilized by conserved hydrogen bonds and van der Waals interactions between acidic residues at the C terminus of domain FN2 and residues N*X*A (where *X* represents Ser, Thr, Gly, or Arg) in a loop in domain FN3 (Fig. 9). We also found interfacial hydrogen bonds and van der Waals interactions in each crystal structure that are only partially conserved in the six CNTNs (supplemental Figs. S5 and S6). Accordingly, we observed distinct conformations at the FN2-FN3 interfaces, but it remains unclear whether these distinct conformations reflect true structural differences or if the FN2-FN3 interface is bent while retaining some flexibility (Fig. 10).

Discussion

Implications for PTPRG and CNTN Signaling—Here we have used biochemical and structural approaches to gain insights into the specific interactions between the protein-tyrosine phosphatase PTPRG and the neural cell adhesion molecules CNTN3–6. Specifically, our results suggest that PTPRG and CNTN3 form *cis*- and *trans*-complexes at the cell surface (Figs. 5*D* and 6), a property that has already been described for certain receptors in the immune system as well as ephrins and Notch/

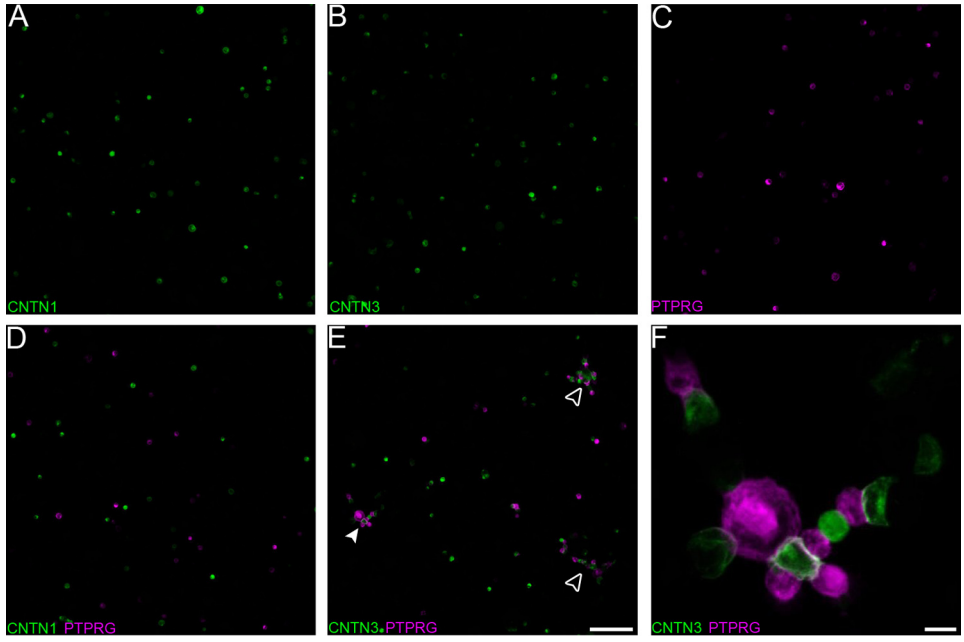

FIGURE 6. **PTPRG and CNTN3 can interact in *trans*.** The ability of PTPRG and CNTN3 to interact in *trans* was assessed using a cell aggregation assay. *A–C*, HEK293F cells grown in suspension were transfected with mEmerald-CNTN1, mEmerald-CNTN3, or mCherry-PTPRG. Cells expressing CNTN1, CNTN3, or PTPRG alone do not form aggregates. Likewise, cellular aggregates do not form when CNTN1- and PTPRG-expressing cells are mixed, consistent with the inability of PTPRG and CNTN1 to interact with one another (*D*). *E*, CNTN3- and PTPRG-expressing cells form aggregates (*white arrowheads*) after the two populations are mixed. *Scale bar*, 100 μm. *F*, *close-up view* of the PTPRG-CNTN3 cell aggregate designated by a *filled arrowhead* in *E*. *Scale bar*, 10 μm.

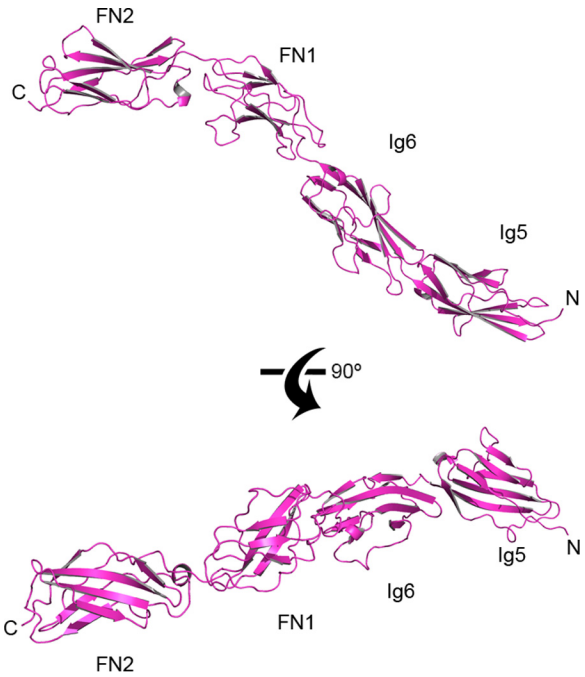

FIGURE 7. **Domains Ig5-FN2 of mouse CNTN3 adopt an extended conformation.** The crystal structure of mouse CNTN3(Ig5-FN2) is shown as a *ribbon diagram*. *N* and *C*, N and C termini, respectively. In the *top view*, domains FN1-FN2 are shown in the same orientation as domains FN1-FN2 in the crystal structure of mouse CNTN3(FN1–FN3) shown in Fig. 8*A*.

Delta (28). Importantly, our structural analyses of CNTN fragments encompassing domains FN1–FN3 are consistent with the hypothesis that CNTNs lie parallel to the cell membrane (Fig. 11). Such an arrangement would be compatible with the formation of both *cis* and *trans* receptor complexes, as was observed in the crystal structure of a Notch·Delta complex (29). In this case, formation of a Notch·Delta *cis*-complex is believed to inhibit Notch signaling, whereas binding of Delta to Notch in *trans* activates Notch signaling. Similarly, ephrins can interact in *cis* with their cognate receptors to dampen the intensity of ephrin-mediated signaling, which is believe to contribute to appropriate guidance of spinal motor axons (30). Thus, it is tempting to speculate that a possible role for *cis*-PTPRG·CNTN3–6 complexes might be to compete with the association of PTPRG and CNTN3–6 in *trans* to fine-tune the intensity of CNTN-mediated signaling through PTPRG.

On the other hand, we have also found that the *cis*-PTPRG·CNTN3 complex is present at the surface of the outer segments of rod photoreceptors. Outer segments do not contact one another but rather are embedded in folds of membranes synthesized by retinal pigment epithelium cells as well as in the interphotoreceptor matrix, a specialized extracellular matrix produced by retinal pigment epithelium cells. Thus, our findings raise three distinct possibilities: 1) the *cis*-complex of PTPRG and CNTN3 is an active signaling unit, 2) a protein found in the interphotoreceptor matrix and/or the retinal pigment epithelium might inhibit the binding of PTPRG to CNTN3 to elicit changes in downstream tyrosine phosphorylation, or 3) a protein found in the interphotoreceptor matrix and/or retinal pigment epithelium cells might associate with the *cis*-PTPRG·CNTN3 complex to form a ternary complex.

Although this remains speculative, we favor the latter possibility because CNTNs form multipartite signaling complexes (*e.g.* a *cis*-complex of CNTN1 and CNTN-associated protein 1 (CNTNAP1) on the axolemma binding to a glial form of neurofascin (31)). More recently, it was shown that a *cis*-complex of CNTN5-CNTNAP4 associates with NrCAM and CHL1 during the formation of specialized presynapses in mouse spinal cords

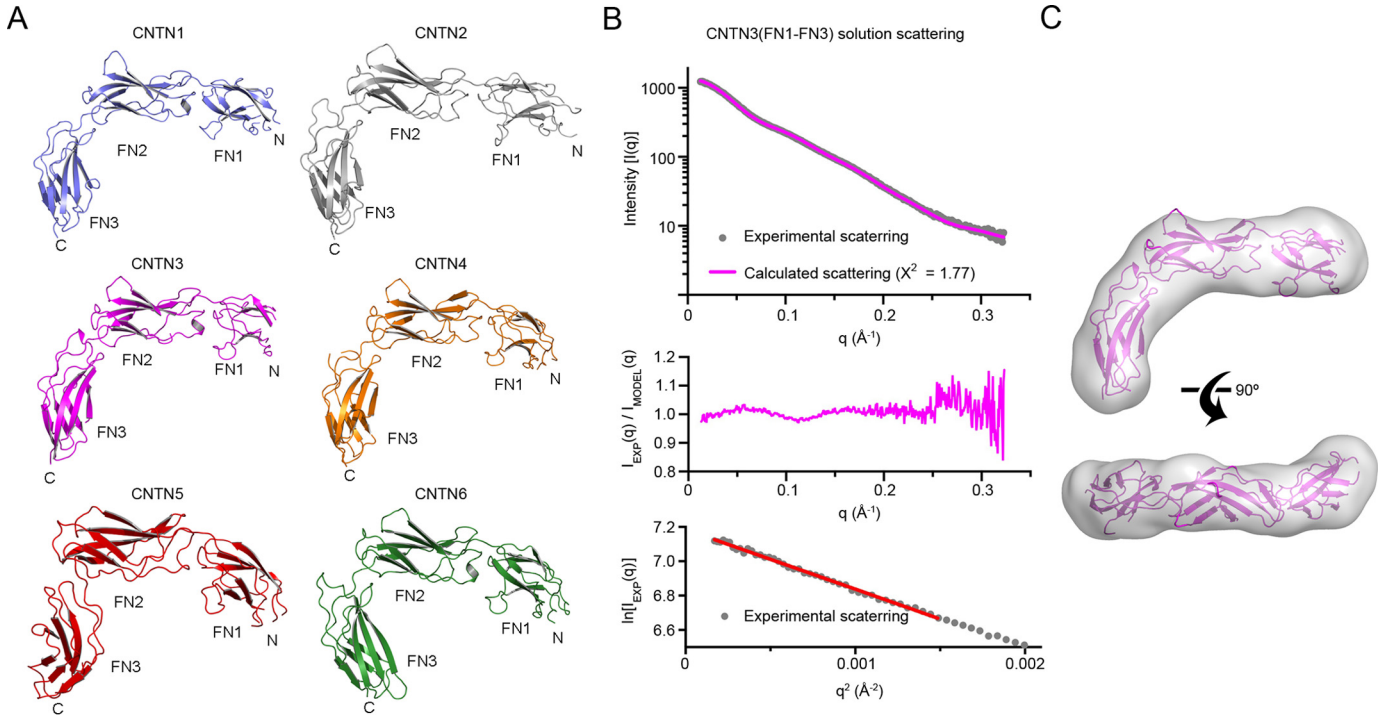

FIGURE 8. **The FN1–FN3 regions of CNTN family members adopt similar bent conformations.** *A*, *ribbon diagrams* of CNTN1–6(FN1-FN3) crystal structures. Residues from CNTN1–6 are *colored* in *slate*, *gray*, *magenta*, *orange*, *red*, and *dark green*, respectively. *B*, small angle x-ray scattering analysis of CNTN3(FN1–FN3). The experimental scattering profile (*gray*) and the theoretical scattering (*magenta line*, $\chi^2 = 1.77$) calculated from the CNTN3(FN1–FN3) crystal structure. Residuals from the fitting of the experimental and scattering profiles are shown *below*. The *bottom panel* shows the Guinier plot with linear fit in *red*. *C*, the crystal structure of CNTN3(FN1–FN3) corresponds to a molecular envelope calculated from the experimental solution scattering profile CNTN3(FN1–FN3) shown in *B*.

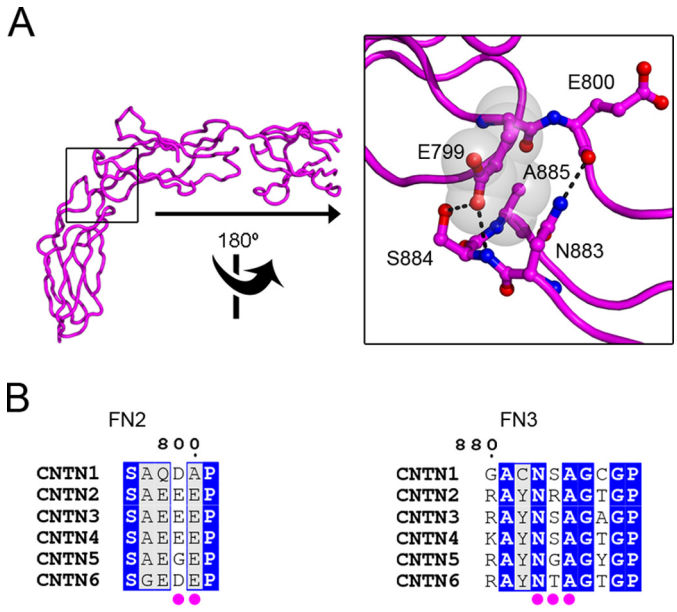

FIGURE 9. **Conserved amino acid contacts at the FN2-FN3 interface.** *A*, the structure of CNTN3(FN1–FN3) is shown as a tube along with a detailed view of the conserved interactions at the FN2-FN3 interface. *Translucent gray spheres* and *black dotted lines* denote van der Waals contacts and potential hydrogen bonds, respectively. *B*, an alignment of mouse CNTN sequences indicates that the contact amino acids at the FN2-FN3 interface shown in *A* are conserved in CNTN family members. Identical amino acids are *shaded* in *blue*, whereas similar residues are *colored light gray*. The *numbering* corresponds to the mouse CNTN3 sequence. *Magenta dots below* the alignments denote residues at the FN2-FN3 interface. See supplemental Figs. S5 and S6.

(32). Finally, a *cis*-complex of CNTN6 and CHL1 controls the oriented growth of dendrites in the neocortex via interaction on the same cell with a RPTP called PTPRA (33). Thus, PTPRG might function as a co-receptor for CNTN3–6 to help transduce signals that these GPI-anchored proteins are unable to relay. Such a possibility would be consistent with our results showing that PTPRG binds to CNTN3–6 in essentially identical fashion. These PTPRG·CNTN co-receptors might associate with known CNTN-binding partners, such as L1 family members, CNTNAPs, or amyloid precursor proteins (8, 11, 32, 34, 35). Targets of PTPRG·CNTN co-receptor complexes might also include yet to be identified proteins that have weak affinities for either PTPRG or a given CNTN but would associate with a PTPRG·CNTN co-receptor complex to form a holoreceptor in much the same way that semaphorins, neuropilins, and plexins do (36).

A Possible Role for PTPRG in Photoreceptors?—PTPRG is expressed in several retinal layers and in particular in the OSs of photoreceptors (Fig. 5) (16). Notably, *Ptprg* null mice do not exhibit any morphological defect in retinas, suggesting that PTPRG is not necessary for retinal development (16). However, previous studies have shown that rod cyclic nucleotide-gated (CNG) channels in the outer segments can be modulated by phosphorylation of a specific tyrosine residue (Tyr^{498}) located in the cyclic nucleotide-binding domain of the α-subunit of the channel protein (37, 38). In addition, release of insulin growth factor I by the retinal pigment epithelium triggers a signaling cascade that eventually leads to the dephosphorylation of CNG channels and modulation of rod light responses by increasing the cGMP sensitivity of CNG channels (39). This raises the possibility that additional tyrosine phosphorylation-dependent mechanisms might alter the light response of photoreceptors. As such, modifications of the PTPRG phosphatase activity

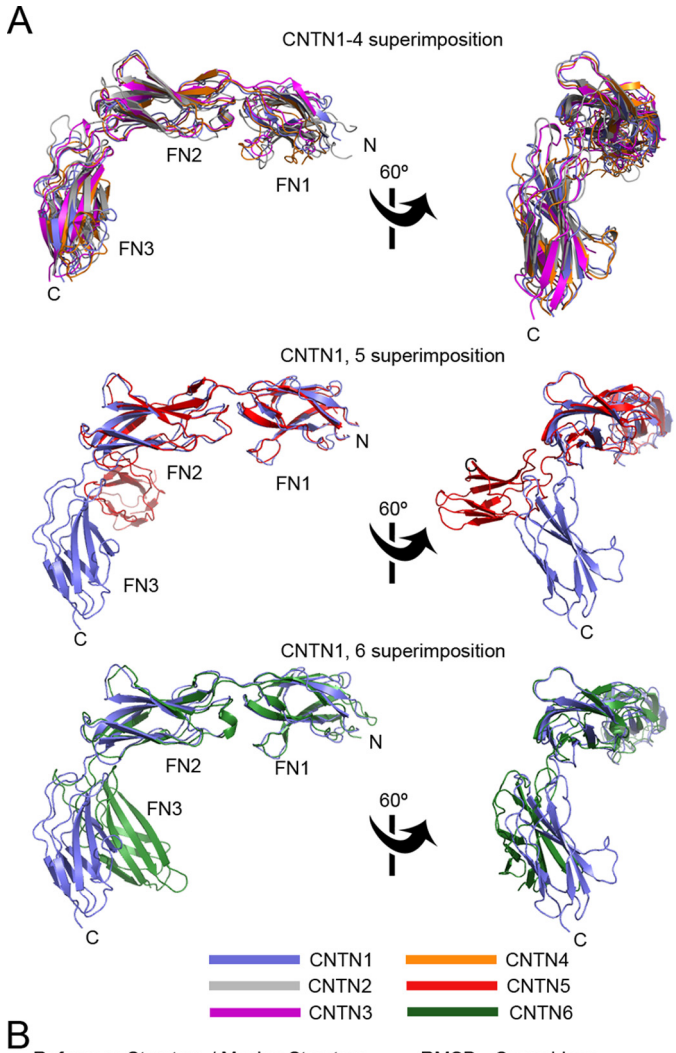

B

Reference Structure / Moving Structure	RMSD - Cα residues
CNTN1(FN1-FN2) / CNTN2(FN1-FN2)	2.36 Å - 188 positions
CNTN1(FN1-FN2) / CNTN3(FN1-FN2)	1.15 Å - 175 positions
CNTN1(FN1-FN2) / CNTN4(FN1-FN2)	2.62 Å - 190 positions
CNTN1(FN1-FN2) / CNTN5(FN1-FN2)	1.91 Å - 189 positions
CNTN1(FN1-FN2) / CNTN6(FN1-FN2)	2.00 Å - 190 positions

FIGURE 10. **Superposition of the FN1-FN2 regions of CNTNs.** *A*, the FN1-FN2 domains of mouse CNTN2, -3, -4, -6, and human CNTN5 were overlaid on the corresponding region of CNTN1. The results are shown in three distinct panels for clarity. Overall, these comparisons indicate that there is significant flexibility in the orientation of domain FN3 with regard to the FN1-FN2 domains. *B*, summary of the superposition details.

upon binding to CNTN3 might provide an additional means to fine-tune phototransduction in the OS. Further investigations designed to probe the role of PTPRG in phototransduction appear warranted.

Adaptation to Restricted Intercellular Spaces—An additional aspect of our work is that it explains how CNTNs might fit within limited extracellular spacing. Indeed, CNTN1 mediates adhesion between axons and myelinating glia and in particular is found at paranodes, which directly flank the nodes of Ranvier. Paranodes are characterized by septate-like junctions between axons and glia where the intermembrane spacing is ~75 Å (40). This limited intercellular space is incompatible with CNTN1 adopting a fully extended conformation because such a molecule would measure ~320 Å if one considers the long axis of a

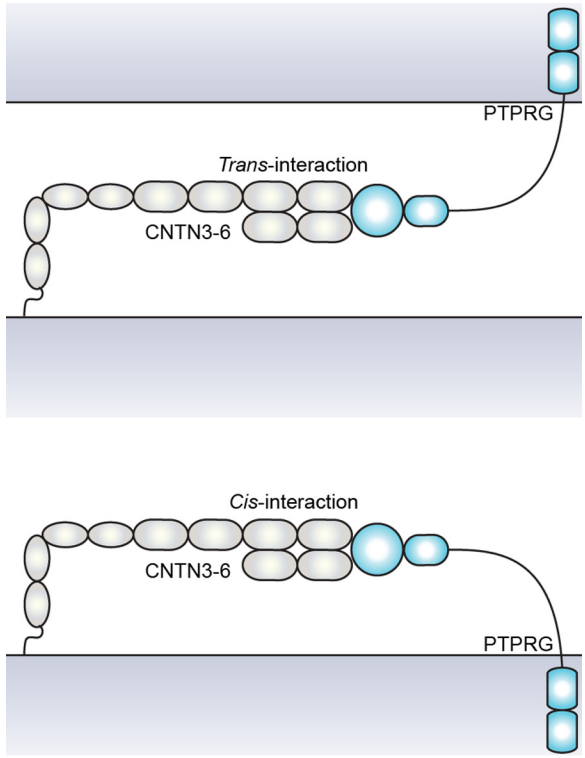

FIGURE 11. **A model illustrating how the conformations of PTPRG and CNTN3–6 could accommodate the formation of *cis*- or *trans*-complexes without altering the interactions between Ig2-Ig3 of CNTNs and the CA domain of PTPRG.**

single Ig or FN domain to be ~40 Å. Thus, a CNTN1 molecule bent at the FN2-FN3 interface might be more adapted to these specialized cell junctions. Similarly, these findings are consistent with the reported roles of CNTN5 and CNTN6 in the formation of synapses during hippocampal formation (14, 35). The distance between the presynaptic membrane, where CNTN5 and -6 are located, and the postsynaptic membrane is ~200 Å, which would also prevent these proteins from adopting an extended conformation.

Experimental Procedures

Protein Expression and Purification—Mouse CNTN5(Ig1–Ig4) was expressed transiently in *N*-acetylglucosaminyltransferase I-negative HEK293S cells, purified, and deglycosylated as described earlier (7). Full-length mouse CNTN1, -3, -4, -5, and -6 fused to human IgG Fc were expressed transiently in HEK293 cells and purified by protein A affinity chromatography. Eluted proteins were >95% pure as judged by SDS-PAGE. Mouse CNTN3(Ig2-Ig3) and mouse CNTN6(Ig2-Ig3) were expressed as hexahistidine fusion proteins in *Escherichia coli* strain T7 Shuffle Express (New England Biolabs). Proteins were purified by metal affinity, ion exchange, and size exclusion chromatographies. The expression of human and mouse PTPRG(CA) as well as human PTPRZ(CA) has been described previously (7). cDNAs mutants of PTPRG(CA) and PTPRZ(CA) were generated by PCR and subcloned into a modified pET32 plasmid (Novagen) that directs the expression of thioredoxin, a hexahistidine tag, a human rhinovirus 3C protease cleavage site, and the protein of interest. These mutants

include mouse PTPRG(CA) and human PTPRZ(CA) with a C-terminal cysteine residue for biotinylation as well as forms of PTPRG(CA) that include mutations in the CNTN-binding regions: 1) H226A/K229A, 2) H295A/V296A, and 3) a deletion in which residues ^{291}EQQDHVKSV^{299} in the β-hairpin are replaced by ASA. The structural integrity of the H226A/K229A and H295A/V296A mutants was evaluated using circular dichroism. Samples of purified wild type PTPRG(CA) and the two site-directed mutants were prepared in PBS (pH 7.4) to a final concentration of 0.2 mg/ml protein. Spectra were recorded from 260 to 190 nm in scanning mode using a Jasco J-815 spectropolarimeter, with a 1-nm bandwidth and a scan rate of 50 nm/min. A total of five replicates were collected and averaged prior to Savitzky-Golay smoothing, using software provided by the manufacturer. Because these spectra were not collected under a vacuum, all data from wavelength values <200 nm should be considered with caution. To generate biotinylated proteins, mouse PTPRG(CA) and human PTPRZ(CA) with a C-terminal cysteine were incubated with EZ-Link maleimide-PEG2-Biotin (Pierce) according to the manufacturer's instructions. Biotinylated proteins were subsequently purified by gel filtration. FN1–FN3 fragments from chick CNTN1, human CNTN5, and mouse CNTN2, -3, -4, and -6 were expressed using as hexahistidine fusion proteins in *E. coli* strain BL21(DE3). Proteins were purified as described above. Selenomethionine-labeled mouse CNTN2(FN1–FN3) was obtained using the same protocol, except for the use of B834(DE3) cells instead of BL21(DE3) cells (41).

Crystallization, Structure Determination, and Structural Analyses—All crystals were grown at 20 °C by hanging drop vapor diffusion. X-ray diffraction data were collected at beamlines 22-BM and 22-ID of the Advanced Photon source facility of Argonne National Laboratory and processed with HKL2000 (42). See supplemental Table S2 for detailed crystallization and freezing conditions. The crystal structures of mouse CNTN5 (Ig1–Ig4) and the complexes of mouse CNTN3(Ig2-Ig3) and mouse CNTN6(Ig2-Ig3) bound to the CA domain of PTPRG were solved by molecular replacement using the relevant chains in the complex of PTPRG and CNTN4(Ig1–Ig4) as search models in PHASER (43) as implemented in PHENIX (44). Final models were obtained after several rounds of manual building in COOT (45) and refinement in PHENIX. Initial attempts to solve the crystal structures of mouse CNTN3(Ig5-FN2) and CNTN3(FN1–FN3) by molecular replacement were not successful. *De novo* phasing using selenomethionine-labeled proteins was not possible because mouse CNTN3(FN1-FN3) does not include any methionine residue. Furthermore, although mouse CNTN3(Ig5-FN2) includes 9 methionine residues located all in Ig5 and Ig6, labeling with selenomethionine was difficult because the protein was expressed in non-methionine auxotroph Origami2(DE3) cells. Finally, heavy metal soaks did not yield any useful crystal derivative. Thus, it was decided to leverage the presence of 7 methionine residues in mouse CNTN2(FN1–FN3) to solve its crystal structure by experimental phasing using anomalous selenium scattering and then use it as a search model for molecular replacement. The initial model for the FN1–FN3 fragment of mouse CNTN2 was obtained by single-wavelength anomalous diffraction using data collected from a crystal grown with selenomethionine-labeled protein using the PHENIX AutoSol and AutoBuild routines. The BAYES correlation coefficient and figure of merit for the solution were 45.6 ± 20.4 and 0.25, respectively. The final refined model was then used as search model to determine the structures of mouse CNTN3(Ig5-FN2), CNTN3(FN1-FN3), and the FN1–FN3 fragments of CNTN1, -4, -5, and -6. Models were validated for Ramachandran statistics and geometry on the RSCB Protein Data Bank validation server. Structures were superimposed using by the DaliLite server (46). Interface areas and contact residues characterized using the PISA server and CCP4, respectively (47, 48). Shape complementarity coefficients were calculated with the program SC (49). Structural representations were generated using PyMol.

AlphaScreen Binding Assays—AlphaScreen binding assays (PerkinElmer Life Sciences) were used to characterize the interactions between PTPRG/Z and their CNTN-binding partners. This assay is based on inhibiting the signal obtained for the interaction of a biotinylated protein bound to streptavidin-coated donor beads and a second target protein bound to protein A-coated acceptor beads. The beads used in the assay were obtained from an AlphaScreen general IgG (Protein A) detection kit. Reactions (25-μl final volume) were initially set up in sealed 96-well microplates to prevent evaporation. Assays were initiated by mixing 5 μl of biotinylated mouse PTPRG(CA) (5 nM final concentration) with 5 μl of either mouse CNTN3, -4, -5, or -6 expressed as human IgG Fc fusion proteins in each well (0.5 nM final concentration). Aliquots (5 μl) of untagged, wild-type PTPRG(CA) of varying concentrations were added to the reactions. Protein A-coated acceptor beads (5 μl, 20 μg/ml final concentration) were then added to each well. After a 1-h incubation at room temperature, streptavidin-coated donor beads (5 μl, 20 μg/ml final concentration) were added to each well. The reactions were allowed to stand at room temperature for 30 min prior to transfer to 96-well half-area opaque microplates for detection using an EnSpire multimode plate reader (PerkinElmer Life Sciences). Values for normalized binding were calculated by dividing the signal measured for a reaction without inhibitor. Results were fitted to a one-site competition equation, in which the IC_{50} is the concentration of inhibitor that gives 50% inhibition of maximal binding using GraphPad Prism (GraphPad Software Inc., La Jolla, CA). The values of IC_{50} are reported as averages ± S.D. from at least three experiments (supplemental Table S1).

Cell-binding Assays—HEK293 cells were maintained in DMEM high glucose supplemented with 10% (v/v) fetal bovine serum. GPI-anchored mouse CNTNs were transiently expressed in HEK293 cells as fusion proteins with human growth hormone as described previously (7). A fragment of human PTPRG including its CA and FN domains fused to human IgG Fc was incubated in the presence of fluorescein isothiocyanate-labeled anti-human Fc antibodies (Jackson) for 30 min. The labeled PTPRG was added to the transfected cells for 15 min in DMEM/F-12 containing 1% N_2 at room temperature and then fixed in 4% (w/v) paraformaldehyde (PFA) in PBS for 10 min. The presence of transfected proteins was detected by immunostaining against human growth hormone using a rabbit poly-

clonal antibody (1:1,000; Fitzgerald, catalogue no. 20R-GR018) (7, 50).

Immunostaining of Mouse Adult Retinas and Proximity Ligation Assays—Retinas were obtained from adult C57BL6 mice (>8 weeks old) from the Jackson Laboratory. All studies followed the guidelines prescribed by the University of Missouri-Kansas City, the institutional care and use committee, and the NEI, National Institutes of Health. Adult mice were deeply anesthetized with CO_2, eyes were enucleated, and the cornea and lens were removed. All eyecups were rapidly fixed for 15 min in 4% (w/v) PFA and processed as described previously for immunohistochemistry (51). Solitary rod photoreceptors were dissociated from isolated retina as described previously (52) and fixed for 10 min in 4% (w/v) PFA, washed in PBS, and processed for indirect immunofluorescence or DuoLink™ analysis.

All tissue was labeled using the indirect immunofluorescence technique using goat anti-CNTN3 (1:200; R&D Systems, catalogue no. AF5339) and mouse anti-PTPRG (1:80; Novus Biologicals, catalogue no. NBPI-02517) as described previously (51). The primary antibody·antigen complexes were detected using secondary antibodies conjugated to CF488 and CF568 (Biotium). *In situ* PLAs were performed to detect *in vivo* interactions between PTPRG and CNTN3 using the primary antibodies and dilutions mentioned above. Retinas were labeled using DuoLink™ *in situ* reagents from Olink Bioscience according to the manufacturer's instructions. A fluorescent signal is obtained when the labeled proteins are within 400 Å of one another. In a control experiment, the primary antibody against CNTN3 was omitted to rule out spurious nonspecific labeling. All images were acquired sequentially using a Nikon C2 confocal microscope with appropriate lasers for excitation (488 and 561 nm) and filters (505–530 nm and 565–600 nm bandpass, respectively). Images were processed for publication using Fiji (53).

Cell Aggregation Assays—cDNAs encoding full-length mouse CNTN1, CNTN3, and PTPRG without their signal sequences were cloned into the mammalian expression vectors pSmEmerald (CNTN1 and -3) and pSmCherry (PTPRG) designed in the laboratory. These vectors derive from the pLEXm plasmid (54) and direct the expression of the chicken PTPRS signal sequence followed by a monomeric Emerald or monomeric Cherry fluorescent protein and the protein of interest. HEK293F cells (ThermoFisher Scientific) were grown in suspension in FreeStyle™ 293 expression medium. Cells (10^7 at a density of 10^6 cells/ml) were transfected using a mixture 10 μg of plasmid and 30 μg of polyethyleneimine-HCl MAX, M_r 40,000 (Polysciences, Inc.) (55). Two days after transfection, $\sim 5 \times 10^6$ cells were spun, washed once with Hanks' balanced salt solution, and resuspended into Hanks' balanced salt solution supplemented with 1% (v/v) fetal bovine serum and 10 mM Na-HEPES, pH 7.5, to a final density of 5×10^5 cells/ml and briefly vortexed. Cell aggregation was initiated by mixing an equal amount of cells into a microcentrifuge tube (final volume 1 ml) and incubating at room temperature with constant agitation. After a 45-min incubation, a 0.5-ml aliquot of the reaction was transferred to a poly-D-lysine-coated glass coverslip. Cells were allowed to attach for 20 min. The cell suspension was then removed, and the coverslip was washed once with PBS. Cells were fixed with 4% (w/v) PFA, washed with PBS, and mounted. Confocal images were acquired sequentially on an Olympus BX61WI with appropriate lasers for excitation (488 and 543 nm) and filters (502–538 nm and 604–644 nm bandpass, respectively) using a DP30BW cooled CCD camera. Images were processed for publication using Fiji (53).

Small Angle X-ray Scattering—SAXS data were collected at the ALS beamline 12.3.1 at Lawrence Berkeley National Laboratory (56). The wavelength λ and the sample-to-detector distances were set to 1.03 Å and 1.5 meters, respectively, resulting in scattering vectors q ranging from 0.01 to 0.32 $Å^{-1}$. The scattering vector is defined as $q = 4\pi \sin\theta/\lambda$, where 2θ is the scattering angle. All experiments were performed at 20 °C, and data were processed as described (56). Data acquired for 0.5, 1, and 2s were merged for calculations using the entire scattering profile. The protein was prepared by size exclusion chromatography on a Superdex 200 10/30 HR column (GE Healthcare) equilibrated in 20 mM Tris-HCl, pH 8.0, 200 mM NaCl prior to data collection. The experimental SAXS data for different protein concentrations were analyzed for aggregation using Guinier plots (57). The radius of gyration (R_g) is 30.9 Å and was derived by the Guinier approximation $I(q) = I(0) \exp(-q^2R_g^2/3)$ with the limits $qR_g < 1.6$ (Fig. 8*B*). The theoretical SAXS profile and the corresponding fit to the experimental data were calculated using the program FoXS (58). A molecular envelope for CNTN3(FN1–FN3) was calculated from the experimental scattering data using the program DAMMIF and averaged using DAMAVER (59, 60). The molecular envelope and the crystal structure of CNTN3(FN1–FN3) were superimposed using Chimera (University of California, San Francisco, CA) (61).

Author Contributions—R. M. N. designed, performed, and analyzed the experiments shown in Figs. 1 (*C* and *D*), 2, 3, 4, 7, 8*A*, 9, and 10. M. H. collected and analyzed the SAXS data in Fig. 8, *B* and *C*. V. D. and S. H. designed, performed, and analyzed the experiments of Fig. 1*B*. R. Z. and S. L. S. designed, performed, and analyzed the experiments of Fig. 5. D. R. H., N. M., and S. J. K. provided technical assistance for the purification of the proteins characterized herein. S. B. designed and coordinated the study and performed the experiments shown in Fig. 6. R. M. N. and S. B. wrote the manuscript. All authors reviewed the results and approved the final version of the manuscript.

Acknowledgments—We thank Prof. Brian Geisbrecht for helpful comments on the manuscript and assistance with circular dichroism. Use of the Advanced Photon Source was supported by the United States Department of Energy, Office of Science, Office of Basic Energy Sciences, under Contract W-31-109-Eng-38. Data were collected at Southeast Regional Collaborative Access Team beamlines at the Advanced Photon Source, Argonne National Laboratory. Supporting institutions may be found at www.ser-cat.org/members.html. X-ray scattering technologies at the Lawrence Berkeley National Laboratory SIBYLS beamline of the Advanced Light Source are supported in part by the United States Department of Energy Program Integrated Diffraction Analysis Technologies (IDAT) and National Institutes of Health Grant MINOS GM105404. Chimera was developed by the Resource for Biocomputing, Visualization, and Informatics at the University of California, San Francisco (supported by NIGMS, National Institutes of Health, Grant P41-GM103311).

References

1. Ensslen-Craig, S. E., and Brady-Kalnay, S. M. (2004) Receptor protein tyrosine phosphatases regulate neural development and axon guidance. *Dev. Biol.* **275,** 12–22
2. Williams, M. E., de Wit, J., and Ghosh, A. (2010) Molecular mechanisms of synaptic specificity in developing neural circuits. *Neuron* **68,** 9–18
3. Harroch, S., Palmeri, M., Rosenbluth, J., Custer, A., Okigaki, M., Shrager, P., Blum, M., Buxbaum, J. D., and Schlessinger, J. (2000) No obvious abnormality in mice deficient in receptor protein tyrosine phosphatase β. *Mol. Cell. Biol.* **20,** 7706–7715
4. Lamprianou, S., Vacaresse, N., Suzuki, Y., Meziane, H., Buxbaum, J. D., Schlessinger, J., and Harroch, S. (2006) Receptor protein tyrosine phosphatase γ is a marker for pyramidal cells and sensory neurons in the nervous system and is not necessary for normal development. *Mol. Cell. Biol.* **26,** 5106–5119
5. Lamprianou, S., Chatzopoulou, E., Thomas J.-L., Bouyain, S., and Harroch, S. (2011) A complex between contactin-1 and the protein tyrosine phosphatase PTPRZ controls the development of oligodendrocyte precursor cells. *Proc. Natl. Acad. Sci. U.S.A.* **108,** 17498–17503
6. Lorenzetto, E., Moratti, E., Vezzalini, M., Harroch, S., Sorio, C., and Buffelli, M. (2014) Distribution of different isoforms of receptor protein tyrosine phosphatase γ (Ptprg-RPTP γ) in adult mouse brain: upregulation during neuroinflammation. *Brain Struct. Funct.* **219,** 875–890
7. Bouyain, S., and Watkins, D. J. (2010) The protein tyrosine phosphatases PTPRZ and PTPRG bind to distinct members of the contactin family of neural recognition molecules. *Proc. Natl. Acad. Sci. U.S.A.* **107,** 2443–2448
8. Shimoda, Y., and Watanabe, K. (2009) Contactins: emerging key roles in the development and function of the nervous system. *Cell Adh. Migr.* **3,** 64–70
9. Zuko, A., Bouyain, S., van der Zwaag, B., and Burbach, J. P. H. (2011) Contactins: structural aspects in relation to developmental functions in brain disease. *Adv. Protein Chem. Struct. Biol.* **84,** 143–180
10. Yamagata, M., and Sanes, J. R. (2012) Expanding the Ig superfamily code for laminar specificity in retina: expression and role of contactins. *J. Neurosci.* **32,** 14402–14414
11. Osterhout, J. A., Stafford, B. K., Nguyen, P. L., Yoshihara, Y., and Huberman, A. D. (2015) Contactin-4 mediates axon-target specificity and functional development of the accessory optic system. *Neuron* **86,** 985–999
12. Kaneko-Goto, T., Yoshihara, S., Miyazaki, H., and Yoshihara, Y. (2008) BIG-2 mediates olfactory axon convergence to target glomeruli. *Neuron* **57,** 834–846
13. Toyoshima, M., Sakurai, K., Shimazaki, K., Takeda, Y., Shimoda, Y., and Watanabe, K. (2009) Deficiency of neural recognition molecule NB-2 affects the development of glutamatergic auditory pathways from the ventral cochlear nucleus to the superior olivary complex in mouse. *Dev. Biol.* **336,** 192–200
14. Sakurai, K., Toyoshima, M., Takeda, Y., Shimoda, Y., and Watanabe, K. (2010) Synaptic formation in subsets of glutamatergic terminals in the mouse hippocampal formation is affected by a deficiency in the neural cell recognition molecule NB-3. *Neurosci. Lett.* **473,** 102–106
15. Yoshihara, Y., Kawasaki, M., Tani, A., Tamada, A., Nagata, S., Kagamiyama, H., and Mori, K. (1994) BIG-1: a new TAG-1/F3-related member of the immunoglobulin superfamily with neurite outgrowth-promoting activity. *Neuron* **13,** 415–426
16. Horvat-Bröcker, A., Reinhard, J., Illes, S., Paech, T., Zoidl, G., Harroch, S., Distler, C., Knyazev, P., Ullrich, A., and Faissner, A. (2008) Receptor protein tyrosine phosphatases are expressed by cycling retinal progenitor cells and involved in neuronal development of mouse retina. *Neuroscience* **152,** 618–645
17. Tolbert, W. D., Daugherty, J., Gao, C., Xie, Q., Miranti, C., Gherardi, E., Vande Woude, G., and Xu, H. E. (2007) A mechanistic basis for converting a receptor tyrosine kinase agonist to an antagonist. *Proc. Natl. Acad. Sci. U.S.A.* **104,** 14592–14597
18. Söderberg, O., Gullberg, M., Jarvius, M., Ridderstråle, K., Leuchowius, K.-J., Jarvius, J., Wester, K., Hydbring, P., Bahram, F., Larsson, L.-G., and Landegren, U. (2006) Direct observation of individual endogenous protein complexes *in situ* by proximity ligation. *Nat. Methods* **3,** 995–1000
19. Hayashi, M., Majumdar, A., Li, X., Adler, J., Sun, Z., Vertuani, S., Hellberg, C., Mellberg, S., Koch, S., Dimberg, A., Koh, G. Y., Dejana, E., Belting, H.-G., Affolter, M., Thurston, G., *et al.* (2013) VE-PTP regulates VEGFR2 activity in stalk cells to establish endothelial cell polarity and lumen formation. *Nat. Commun.* **4,** 1672
20. Johnson, K. G., Tenney, A. P., Ghose, A., Duckworth, A. M., Higashi, M. E., Parfitt, K., Marcu, O., Heslip, T. R., Marsh, J. L., Schwarz, T. L., Flanagan, J. G., and Van Vactor, D. (2006) The HSPGs Syndecan and Dallylike bind the receptor phosphatase LAR and exert distinct effects on synaptic development. *Neuron* **49,** 517–531
21. Coles, C. H., Shen, Y., Tenney, A. P., Siebold, C., Sutton, G. C., Lu, W., Gallagher, J. T., Jones, E. Y., Flanagan, J. G., and Aricescu, A. R. (2011) Proteoglycan-specific molecular switch for RPTPσ clustering and neuronal extension. *Science* **332,** 484–488
22. Parent, A.-S., Mungenast, A. E., Lomniczi, A., Sandau, U. S., Peles, E., Bosch, M. A., Rønnekleiv, O. K., and Ojeda, S. R. (2007) A contactin-receptor-like protein tyrosine phosphatase β complex mediates adhesive communication between astroglial cells and gonadotrophin-releasing hormone neurones. *J. Neuroendocrinol.* **19,** 847–859
23. Barnea, G., Silvennoinen, O., Shaanan, B., Honegger, A. M., Canoll, P. D., D'Eustachio, P., Morse, B., Levy, J. B., Laforgia, S., and Huebner, K. (1993) Identification of a carbonic anhydrase-like domain in the extracellular region of RPTP γ defines a new subfamily of receptor tyrosine phosphatases. *Mol. Cell. Biol.* **13,** 1497–1506
24. Coles, C. H., Mitakidis, N., Zhang, P., Elegheert, J., Lu, W., Stoker, A. W., Nakagawa, T., Craig, A. M., Jones, E. Y., and Aricescu, A. R. (2014) Structural basis for extracellular *cis* and *trans* RPTPσ signal competition in synaptogenesis. *Nat. Commun.* **5,** 5209
25. Kulahin, N., Kristensen, O., Rasmussen, K. K., Olsen, L., Rydberg, P., Vestergaard, B., Kastrup, J. S., Berezin, V., Bock, E., Walmod, P. S., and Gajhede, M. (2011) Structural model and *trans*-interaction of the entire ectodomain of the olfactory cell adhesion molecule. *Structure* **19,** 203–211
26. Chen, F., Venugopal, V., Murray, B., and Rudenko, G. (2011) The structure of neurexin 1α reveals features promoting a role as synaptic organizer. *Structure* **19,** 779–789
27. Miller, M. T., Mileni, M., Comoletti, D., Stevens, R. C., Harel, M., and Taylor, P. (2011) The crystal structure of the α-neurexin-1 extracellular region reveals a hinge point for mediating synaptic adhesion and function. *Structure* **19,** 767–778
28. Held, W., and Mariuzza, R. A. (2011) *Cis-trans* interactions of cell surface receptors: biological roles and structural basis. *Cell Mol. Life Sci.* **68,** 3469–3478
29. Luca, V. C., Jude, K. M., Pierce, N. W., Nachury, M. V., Fischer, S., and Garcia, K. C. (2015) Structural basis for Notch1 engagement of Delta-like 4. *Science* **347,** 847–853
30. Kao, T.-J., and Kania, A. (2011) Ephrin-mediated cis-attenuation of Eph receptor signaling is essential for spinal motor axon guidance. *Neuron* **71,** 76–91
31. Charles, P., Tait, S., Faivre-Sarrailh, C., Barbin, G., Gunn-Moore, F., Denisenko-Nehrbass, N., Guennoc, A.-M., Girault, J.-A., Brophy, P. J., and Lubetzki, C. (2002) Neurofascin is a glial receptor for the paranodin/Caspr-contactin axonal complex at the axoglial junction. *Curr. Biol.* **12,** 217–220
32. Ashrafi, S., Betley, J. N., Comer, J. D., Brenner-Morton, S., Bar, V., Shimoda, Y., Watanabe, K., Peles, E., Jessell, T. M., and Kaltschmidt, J. A. (2014) Neuronal Ig/Caspr recognition promotes the formation of axoaxonic synapsesin mouse spinal cord. *Neuron* **81,** 120–129
33. Ye, H., Tan, Y. L. J., Ponniah, S., Takeda, Y., Wang, S.-Q., Schachner, M., Watanabe, K., Pallen, C. J., and Xiao, Z.-C. (2008) Neural recognition molecules CHL1 and NB-3 regulate apical dendrite orientation in the neocortex via PTP α. *EMBO J.* **27,** 188–200
34. Osterfield, M., Egelund, R., Young, L. M., and Flanagan, J. G. (2008) Interaction of amyloid precursor protein with contactins and NgCAM in the retinotectal system. *Development* **135,** 1189–1199
35. Shimoda, Y., Koseki, F., Itoh, M., Toyoshima, M., and Watanabe, K. (2012) A *cis*-complex of NB-2/contactin-5 with amyloid precursor-like protein 1 is localized on the presynaptic membrane. *Neurosci. Lett.* **510,** 148–153

36. Janssen, B. J. C., Malinauskas, T., Weir, G. A., Cader, M. Z., Siebold, C., and Jones, E. Y. (2012) Neuropilins lock secreted semaphorins onto plexins in a ternary signaling complex. *Nat. Struct. Mol. Biol.* **19,** 1293–1299
37. Molokanova, E., Trivedi, B., Savchenko, A., and Kramer, R. H. (1997) Modulation of rod photoreceptor cyclic nucleotide-gated channels by tyrosine phosphorylation. *J. Neurosci.* **17,** 9068–9076
38. Molokanova, E., Maddox, F., Luetje, C. W., and Kramer, R. H. (1999) Activity-dependent modulation of rod photoreceptor cyclic nucleotide-gated channels mediated by phosphorylation of a specific tyrosine residue. *J. Neurosci.* **19,** 4786–4795
39. Savchenko, A., Kraft, T. W., Molokanova, E., and Kramer, R. H. (2001) Growth factors regulate phototransduction in retinal rods by modulating cyclic nucleotide-gated channels through dephosphorylation of a specific tyrosine residue. *Proc. Natl. Acad. Sci. U.S.A.* **98,** 5880–5885
40. Nans, A., Einheber, S., Salzer, J. L., and Stokes, D. L. (2011) Electron tomography of paranodal septate-like junctions and the associated axonal and glial cytoskeletons in the central nervous system. *J. Neurosci. Res.* **89,** 310–319
41. Bouyain, S., and Leahy, D. J. (2007) Structure-based mutagenesis of the substrate-recognition domain of Nrdp1/FLRF identifies the binding site for the receptor tyrosine kinase ErbB3. *Protein Sci.* **16,** 654–661
42. Otwinowski, Z., and Minor, W. (1997) Processing of x-ray diffraction data collected in oscillation mode. *Methods Enzymol.* **276,** 307–326
43. McCoy, A. J., Grosse-Kunstleve, R. W., Adams, P. D., Winn, M. D., Storoni, L. C., and Read, R. J. (2007) Phaser crystallographic software. *J. Appl. Crystallogr.* **40,** 658–674
44. Adams, P. D., Afonine, P. V., Bunkóczi, G., Chen, V. B., Davis, I. W., Echols, N., Headd, J. J., Hung, L. W., Kapral, G. J., Grosse-Kunstleve, R. W., McCoy, A. J., Moriarty, N. W., Oeffner, R., Read, R. J., Richardson, D. C., *et al.* (2010) PHENIX: a comprehensive Python-based system for macromolecular structure solution. *Acta Crystallogr. D. Biol. Crystallogr.* **66,** 213–221
45. Emsley, P., and Cowtan, K. (2004) Coot: model-building tools for molecular graphics. *Acta Crystallogr. D Biol. Crystallogr.* **60,** 2126–2132
46. Hasegawa, H., and Holm, L. (2009) Advances and pitfalls of protein structural alignment. *Curr. Opin. Struct. Biol.* **19,** 341–348
47. Krissinel, E., and Henrick, K. (2007) Inference of macromolecular assemblies from crystalline state. *J. Mol. Biol.* **372,** 774–797
48. Winn, M. D., Ballard, C. C., Cowtan, K. D., Dodson, E. J., Emsley, P., Evans, P. R., Keegan, R. M., Krissinel, E. B., Leslie, A. G. W., McCoy, A., McNicholas, S. J., Murshudov, G. N., Pannu, N. S., Potterton, E. A., Powell, H. R., *et al.* (2011) Overview of the CCP4 suite and current developments. *Acta Crystallogr. D Biol. Crystallogr.* **67,** 235–242
49. Lawrence, M. C., and Colman, P. M. (1993) Shape complementarity at protein/protein interfaces. *J. Mol. Biol.* **234,** 946–950
50. Hamaoka, B. Y., Dann, C. E., 3rd, Geisbrecht, B. V., and Leahy, D. J. (2004) Crystal structure of *Caenorhabditis elegans* HER-1 and characterization of the interaction between HER-1 and TRA-2A. *Proc. Natl. Acad. Sci. U.S.A.* **101,** 11673–11678
51. Stella, S. L., Jr., Vila, A., Hung, A. Y., Rome, M. E., Huynh, U., Sheng, M., Kreienkamp, H.-J., and Brecha, N. C. (2012) Association of shank 1A scaffolding protein with cone photoreceptor terminals in the mammalian retina. *PLoS One* **7,** e43463
52. Zayas-Santiago, A., and Kang Derwent, J. J. (2009) Preservation of intact adult rat photoreceptors *in vitro*: study of dissociation techniques and the effect of light. *Mol. Vis.* **15,** 1–9
53. Schindelin, J., Arganda-Carreras, I., Frise, E., Kaynig, V., Longair, M., Pietzsch, T., Preibisch, S., Rueden, C., Saalfeld, S., Schmid, B., Tinevez, J.-Y., White, D. J., Hartenstein, V., Eliceiri, K., Tomancak, P., and Cardona, A. (2012) Fiji: an open-source platform for biological-image analysis. *Nat. Methods* **9,** 676–682
54. Aricescu, A. R., Lu, W., and Jones, E. Y. (2006) A time- and cost-efficient system for high-level protein production in mammalian cells. *Acta Crystallogr. D Biol. Crystallogr.* **62,** 1243–1250
55. Longo, P. A., Kavran, J. M., Kim, M.-S., and Leahy, D. J. (2013) Transient mammalian cell transfection with polyethylenimine (PEI). *Methods Enzymol.* **529,** 227–240
56. Hura, G. L., Menon, A. L., Hammel, M., Rambo, R. P., Poole, F. L., 2nd, Tsutakawa, S. E., Jenney, F. E., Jr., Classen, S., Frankel, K. A., Hopkins, R. C., Yang, S.-J., Scott, J. W., Dillard, B. D., Adams, M. W. W., and Tainer, J. A. (2009) Robust, high-throughput solution structural analyses by small angle x-ray scattering (SAXS). *Nat. Methods* **6,** 606–612
57. Guinier, A., and Fournet, G. (1955) *Small-angle Scattering of X-rays*, Wiley Interscience, New York
58. Schneidman-Duhovny, D., Hammel, M., Tainer, J. A., and Sali, A. (2013) Accurate SAXS profile computation and its assessment by contrast variation experiments. *Biophys. J.* **105,** 962–974
59. Volkov, V. V., and Svergun, D. I. (2003) Uniqueness of *ab initio* shape determination in small-angle scattering. *J. Appl. Crystallogr.* **36,** 860–864
60. Franke, D., and Svergun, D. I. (2009) DAMMIF, a program for rapid *ab-initio* shape determination in small-angle scattering. *J. Appl. Crystallogr.* **42,** 342–346
61. Pettersen, E. F., Goddard, T. D., Huang, C. C., Couch, G. S., Greenblatt, D. M., Meng, E. C., and Ferrin, T. E. (2004) UCSF Chimera: a visualization system for exploratory research and analysis. *J. Comput. Chem.* **25,** 1605–1612